SLAC – PUB – 4122
October 1986
(I)

A Sonar-Based Technique for the Ratiometric Determination of Binary Gas Mixtures*

G. HALLEWELL, G. CRAWFORD,† D. MCSHURLEY,
G. OXOBY, AND R. REIF

Stanford Linear Accelerator Center
Stanford University, Stanford, California, 94305

ABSTRACT

We have developed an inexpensive sonar-based instrument to provide a routine on-line monitor of the composition and stability of several gas mixtures having application in a Čerenkov Ring Imaging Detector. The instrument is capable of detecting small (< 1%) fluctuations in the relative concentration of the constituent gases, and in contrast with some other gas analysis techniques, lends itself well to complete automation.

Submitted to *Nuclear Instruments and Methods*

* Work supported by the Department of Energy, contract DE – AC03 – 76SF00515.
† Present Address: Dept. of Physics, Cornell University, Ithaca, New York 14853, U.S.A.

1. Introduction

As part of the development program for a Čerenkov Ring Imaging Detector (CRID) [1-3] for the SLD experiment [4] at the SLAC Linear Collider (SLC) we have developed a novel technique for analysis of several binary gas mixtures which might be used as the Čerenkov gas radiators and the drift gases of the CRID time projection chambers (TPCs).

A simple sonar instrument makes use of difference in the velocity of sound in various "component" gases to determine their relative concentration in each particular binary mixture.

Particles emerging from interactions at SLC will traverse the SLD CRID, emitting ultraviolet Čerenkov radiation in liquid (perfluoro-n-hexane: C_6F_{14}) and gas (perfluoro-n-pentane: C_5F_{12}) radiators which will be focussed onto an array of quartz window TPCs, to be converted to photoelectrons in the TPC drift gas; a mixture of methane (CH_4) with either ethane (C_2H_6) or isobutane (C_4H_{10}), together with the photoionizing vapor TMAE (Tetrakis-dimethylamino Ethylene, $E_i = 5.34$ eV). Photoelectrons will drift in a uniform electric field up to 1.2 m in the TPCs to be detected at proportional wire planes.

Accurate monitoring and control of the temperature, pressure, composition and impurity levels in the TPC drift gas and the Čerenkov radiators is essential to the stable operation of the CRID. A comprehensive gas monitoring and control system is under development and in this report we discuss one of several monitoring instruments that might be incorporated into it.

2. The CRID Gas Systems

2.1 The TPC Gas Delivery System

This system must deliver a high purity binary mixture of the constituent drift gases in a ratio necessary to set up the desired electron drift velocity in the TPCs. Approximately 0.6 Torr of saturated TMAE vapor will be added to the drift gas mixture [5], as it is bubbled through liquid TMAE maintained at a temperature of 28°C.

At a particular value of drift field, and at constant temperature, pressure and levels of contamination from trace impurities — parameters that themselves require accurate monitoring and control—the velocity of the drifting electrons can change significantly due to small variations in the drift gas mixture ratio.

In our prototype studies we have investigated a variety of TPC gas mixtures. The substitution of ethane for the more electronegative isobutane was accompanied by a significant improvement in the lifetime of drifting electrons, and it is likely that a methane-ethane mix will be chosen for the SLD CRID. We have however made extensive measurements of sound velocity in a variety of possible CH_4/C_4H_{10} and CH_4/C_2H_6 drift gas combinations (§4.2).

The binary drift gas mixture might be supplied in bulk premixed form, or might be volumetrically mixed immediately before use by a pair of mass flow controllers* operating in ratiometric mode. The latter system would allow the concentrations of the two components to be varied at will, selecting a range of drift velocities in the TPCs without recourse to drift field variation. In each case, however, routine verification of the gas mixture is desirable, either as an independent monitor of the premixing of the gases, or of the stability of operation of the mass flow controllers.

2.2 The CRID Gas Radiator System

Although our prototype development [1- 3] has up to now relied on an atmospheric pressure isobutane radiator, the most probable choice for the SLD CRID gas radiator is perfluoro-n-pentane (C_5F_{12}). This material has the desirable property of non-flammability and the relatively high refractive index of ~ 1.0017 at atmospheric pressure ($\lambda \sim 200$ nm). It is, however, very expensive and has a relatively high boiling point of $\sim 30°C$ at atmospheric pressure: disadvantages that demand a recirculating radiator gas flow system completely maintained at a temperature in excess of the boiling point.

* In this context, the term "Mass Flow Controller" is a misnomer. The MFC electronic flowmeter determines the passage of gas from the heat transferred between two electrical filaments, which is closely related to the mass flow. However, internal correction circuitry is used to convert the meter signal into a voltage proportional to volume flow. The necessary correction factors are determined by calibration against a known flow of gas.

Prior to filling with C_5F_{12}, the gas radiator enclosures will be purged of air and water vapor with high purity nitrogen, which will itself be subsequently replaced by C_5F_{12}. The thermodynamic replacement process will extract gas from the radiator vessels, cool it to below the C_5F_{12} boiling temperature and allow any uncondensed gas to escape. During the process, the radiator gas will be maintained at an overpressure of about 2 Torr relative to atmosphere by the addition of more C_5F_{12} until the vessels are almost completely filled with C_5F_{12}. In effect, the partial pressure of C_5F_{12} in the radiator vessel is gradually increased as the nitrogen is replaced. Radiator gas analysis will be required to verify that the nitrogen concentration is less than $\sim$ 1%, thereby maximizing the radiator refractive index to achieve the required low secondary particle momentum thresholds. In the recovery mode, the same analysis system could verify that the C_5F_{12} had been almost completely replaced by nitrogen, allowing the radiator enclosures to be flushed out with air prior to opening.

Since a similar filling and recovery scheme could be used with an isobutane radiator; sound velocity studies have been made in a variety of mixtures of both N_2/C_4H_{10} and N_2/C_5F_{12} (§4.2).

2.3 The Value of Sound Velocity measurements in Simple Gas Analysis

While any of a number of sophisticated analysis techniques–including those listed below–might be applied to the rather simple analysis of a binary gas mixture, these generally require expensive equipment and a high level of operator supervision, neither of which, it will be shown, are necessary with the sonar technique.

1. In our prototype development work we have routinely identified trace contaminants (< 1 part per million) in gas streams by means of gas chromatography (GC). While routine GC studies of SLD CRID gas streams are anticipated, these will be limited to the search for trace impurities—for example electron–absorbing TMAE impurities in the drift gas—inaccessible to other techniques. Although extremely sensitive, GG equipment can exhibit significant drifts in calibration, and requires a high level of operator supervision.
2. While binary gas analysis by thermal conductivity (TC) is common, TC analyzers are usually supplied factory–calibrated for a specific gas pair: conversion and recalibration

for other gases are time consuming and often problematic. Many TC analyzers are unsuitable for use with fluorocarbons since, in the presence of moisture, highly corrosive degradation products can be formed when these gases pass over the hot sensor filaments.

3. The velocity of electron drift in the CRID TPCs is itself a strong function of the drift gas mixture—at constant temperature, pressure, electric field and levels of contamination from trace impurities —but any drift velocity analysis of the TPC gases would require an extensive pre–calibration under identical operating conditions. Furthermore, a second method of analysis would be needed for the radiator gases, since C_5F_{12} is highly electronegative.

4. The relative concentration of the components in a binary gas mixture can be accurately determined from measurements of its refractive index and knowledge of the refractive indices of the individual components under conditions of identical temperature and pressure. These measurements however generally require an expensive optical interferometer and very accurate control by the operator of the temperature and pressure of the gas sent to it.

In comparison with the above techniques, the analysis of gas mixtures by pulse delay (sonar) sound velocity measurement is simple, inexpensive and lends itself well to complete automation, requiring only the measurement of a time interval between the transmitted and received sound pulses, and knowledge of the temperature of the gas in the sonar vessel.

A single sonar tube can furthermore be used to monitor both the CRID radiator gas and drift gas mixture, the gas streams being selected and directed to the tube by means of a series of remote-control valves.

In the narrow CRID operating range around one atmosphere, sound velocity has the important advantage of virtual pressure independence. While sonar analysis of binary gas mixtures can be very simple, requiring no thermodynamic input at all, extensive tabulations of thermodynamic data for nitrogen and the various hydrocarbons have allowed us to make (§4.1, 4.2) very detailed comparisons between our velocity measurements and the predictions of several empirical equations of state of varying complexity. The generally good agreement seen has given us confidence in the accuracy and reproducibility our velocity measurements.

When the equation of state of a gas mixture cannot be accurately calculated—as in the case of C_5F_{12}/N_2 mixtures (§4.2), due to the scarcity of tabulated C_5F_{12} thermodynamic data—the variation of the measured sound velocity with the relative concentrations of the two gases (at fixed temperature) can be used to generate an empirical "look-up table," allowing the gas composition to be deduced from any measured velocity (§4.3).

3. The Ultrasonic Gas Analysis System

3.1 General Description of the Test Apparatus

Figure 1 shows the prototype ultrasonic gas analysis system. The sample gas is admitted to an 8 cm diameter aluminum tube containing two ultrasonic transducers accurately located a known distance apart. The sonar tube has an overall length of about 90 cm and is kept immersed in a uniform temperature liquid bath. Two platinum resistance thermometers monitor the temperature of the gas in the tube. The temperature of the liquid in the bath is controlled by a closed copper heat exchanger circuit through which ethylene glycol is continuously pumped by a recirculating temperature control unit* . The gas inlet line is immersed in the liquid over about 1 m of its length to help bring the sample gas into thermal equilibrium with the sonar tube.

Although the prototype sonar tube is mounted horizontally, a vertical mounting is planned for future use, allowing the unit to be mounted in a compact gas monitoring rack.

Single component gases (except C_5F_{12}) or premixed gases are supplied to the sonar tube through one or other of a pair of mass flow controllers† (MFCs) which also allow mixtures of any desired ratio to be set up. C_5F_{12} is supplied from a small, heated cylinder through piping maintained at a temperature of $> 35°C$. The sonar vessel may be evacuated to allow C_5F_{12}/N_2 combinations to be mixed *in situ* with the aid of a high precision sub-atmospheric pressure gauge* . The ultrasonic transducers have shown no degradation in performance after many such evacuations.

---

* Model RTE-4, Neslab Instruments Inc. Portsmouth, NH, U.S.A.
† Model 1258A, MKS Inc. Burlington, MA, U.S.A.
* Model FA129 Wallace and Tiernan Co. Belleville, NJ, U.S.A.

A monitor manifold allows the input or exhaust gas to be independently monitored by a gas chromatograph[‡] , to verify the mixture in the sonar tube or check the MFC calibration.

Figure 2 is a schematic of the sonar drive and readout electronics. Eight 45 KHz sound pulses are passed through the sample gas to be detected at the receiving transducer. A 4 MHz readout clock is started on the leading edge of the transmitted pulse envelope and is stopped by the amplified and discriminated output of the receiving transducer. The transit time of the sound pulse is then displayed, in units of 250 ns, on a 6 digit display or can be read into a monitoring computer via a simple CAMAC scaler. The sound velocity in the gas is given by

$$V_S = \frac{d}{N \times 250 \times 10^{-9}} \; ms^{-1}$$

where d is the known distance in meters between the transmitting and receiving transducers, and N is the recorded number of readout clock pulses.

3.2 The Transducers and Their Drive and Amplifier Circuits

The major components of the ultrasonic transducer are shown in Fig. 3. The device[♮] [6], originally developed for application in the range finder of an autofocus camera, can be operated both as an electrostatic loudspeaker and microphone.

The insulating side of a 3.8 cm diameter gold coated plastic foil is stretched across a grooved metallic plate to form a capacitor which when charged, exerts an electrostatic force on the foil.

In the transmit mode, the charging effect of the A.C. pulse train produces the sound oscillations. In the receive mode, the transducer is generally operated with a bias voltage of between $+50 \rightarrow +150V$ DC applied to the grooved electrode, the foil being grounded. The net force acting on the foil is modified by an incoming sound wave train, which alters the transducer capacitance to produce an A.C. output signal.

---

‡ Model 8500, Carle Instruments, Hach & Co. Loveland, CO. U.S.A. (With 1/8 inch, 8 ft. "PORAPAC N" and "PORAPAC Q" Column; 50/80 Mesh).

♮ Polaroid Corp. instrument grade transducer, part no. 604142.

The transducer drive circuit is shown in Fig. 4(a). The TTL input pulse train generates eight 160V RMS pulses at the transmitting transducer by switching 6 V DC through the primary of a small transformer[◇] .

Figure 4(b) is a general view of the receiving circuit. The receiving transducer was typically operated at a D.C. bias of +80V and A.C. coupled to a sensitive fast preamplifier[•] followed by a second stage amplifier and discriminator.

3.3 Sources of Error in the Ultrasonic Measurements

Investigations have been made of various systematic effects which might affect the accuracy of the sound velocity determination in single gases and binary mixtures.

The distance between the foils of the two transducers has been measured to an accuracy of $\pm$ 1 mm, or about 0.1% of the path length. It is expected to change by no more than 0.4 mm (0.05%) due to the linear expansion of the aluminum tube over the 20°C measurement range. The platinum resistance thermometers were calibrated before use and were found to deviate from the true temperature by $\leq$ 0.3°C (Table I). The agreement between the two resistance thermometers was good over the whole temperature range, indicating that there were no obvious temperature gradients within the sonar tube.

Correction factors for the confining effects of the sonar tube have been investigated, using the Helmholz-Kirchoff formula (see for example Ref. 7). For all the gases considered in this work, the velocity correction for the 8 cm diameter tube at a sound frequency of 45 KHz was found to be negligible.

Figure 5 shows a typical sonar pulse waveform, seen at the input to the receiving preamplifier (air, + 80V receiver bias). We have observed a wide, though temperature-independent, dynamic range of received signals, varying between a peak-to-peak average of 40 mV in CH_4 to 400 mV in N_2. We accordingly bias the receiving transducer and have, in our prototype sonar, employed a commercial low noise pre-amplifier with a sensitivity typical of PWC applications.

◇ Polaroid Corp. Part No. 605541.

• Model HQV810, LeCroy Corp., West Nyack, NY, U.S.A.

We have studied the dependence of the measured sound velocity on the size of the first detected sound cycle, and estimate the error in measured transit time to be ≤ 5 μs for the gases studied in this work. This represents a worst case error of 0.25% in the velocity for CH_4, the fastest of the pure gases, and we estimate our overall systematic error in velocity measurement to be no more than $\pm$ 0.3% (Table I).

The overall error in the sonar determination of a gas mixture is dependent on the uncertainties in the parameters that define its velocity-composition curve. In fits to empirical measurements, these in turn are dominated by the inaccuracy with which the initial calibration mixtures were set up, either with ratiometric MFCs or by other mixing techniques.

In all MFC-set mixtures, the absolute flows were kept as high as possible to minimize the contribution of the manufacturer's quoted flow error of $\pm$ 0.5% of full scale at any flow. With the exception of C_5F_{12}, calibration tables were drawn up to relate the actual flow$^{\nabla}$ of a particular gas to the MFC output voltage. Even with these precautions we believe from our independent GC measurements and comparison with premixed standards that volumetric gas mixtures set up with the ratiometric MFCs are accurate to an average of no better than $\pm$ 1% (Table I).

With the exception of C_5F_{12} all the gases were supplied by the same manufacturer** and have purities of 99.5% or higher (99.95% for C_2H_6). Generally, the contamination consists of roughly equal amounts of heavier and lighter gases, and has very little effect on the overall sound velocity. For example, an increase of $\sim$ 1 % in the purity of ethane (comparing a 99% purity sample with 99.95%) was found to increase the measured sound velocity by $\leq$ 0.2% over the entire temperature range. Since the gases to be used in the CRID TPCs will be at least 99.9% pure, the velocity spread due to impurities should be no more than $\sim$ 0.02%, which is negligible in comparison with our systematic velocity measurement error of $\pm$ 0.3%

C_5F_{12} was supplied in liquid form with a purity in excess of 99%. The major contaminants, identified in a GC-MS analysis by the manufacturers** , were other isomers of perfluoropentane

∇ Measured with Hewlett-Packard Model 0101-0113 Soap Film Flowmeter.
** Matheson Gas Products Inc., Secaucus, NJ 07094, U.S.A.
** ISC Chemicals Ltd. Avonmonth, Bristol BS11 9HP, U.K.

namely perfluoro-2-methyl butane and perfluoro-mono-methyl-cyclobutane. Other contamination is expected in the form of dissolved impurity gases, particularly air, which re-emerge to contaminate the gaseous phase. Gas solubility data for similar liquid fluorocarbons lead us to expect a volume impurity level of about 0.4%. As the dissolved gases are all much lighter than gaseous C_5F_{12}, their influence on the sound velocity in C_5F_{12} could be significant.

Since the radiator gas recirculation system will essentially operate in a partial pressure replacement mode (§2.2), all C_5F_{12}/N_2 mixtures have been set up by partial pressure. The mixing gauge (§3.1) was calibrated against a high precision capacitance manometer, and we believe that all partial pressure mixtures are accurate to better than $\pm$ 0.5%. We therefore estimate the overall systematic uncertainty in composition for C_5F_{12}/N_2 mixtures to be $\sim \pm 1\%$.

The various systematic errors are summarized in Table I and are used as nominal error bars in Figs. 6-16.

4. The Use of Sound Velocity Measurements in Gas Analysis

In this section we consider some theoretical aspects of sound propagation in single component and binary gases, and compare our velocity measurements with the various theoretical predictions.

We begin (§4.1) by comparing our velocity measurements in single component gases with the predictions made firstly under an ideal gas equation of state, and secondly, under two more realistic empirical equations of state. In our analysis of gas mixtures (§4.2) we compare our velocity measurements with the predictions of three different mixing rules, made under the three equations of state.

We find that although the various theoretical velocity predictions are generally in good agreement (within $\sim$ 3%) with our measurements, each mixing rule or equation of state is limited in its application—often by the availability of the prerequisite thermodynamic data—and cannot satisfactorily predict the sound velocity in all the gas mixtures of CRID interest.

While the free parameters of these empirical formulae might be adjusted to accommodate a wider variety of gases, high accuracy ($\sim$ 1 %) sonar determinations of any particular binary

gas mixture are most easily made at present from a simple polynomial parametrization of the variation of sound velocity with the relative concentration of the two components. Details of the fitting procedure and tabulation of the fit parameters for each gas mixture are given in §4.3.

4.1 The Velocity of Sound in a Single Component Gas

The velocity of sound in any pure gas at a temperature T(Kelvin) is given by [8]

$$V_S = \left[\frac{RT}{M}\left(f + \frac{gR}{C_V}\right)\right]^{\frac{1}{2}} \tag{1}$$

$$\text{where } f = \frac{-V^2}{RT}\left(\frac{\partial P}{\partial V}\right)_T \tag{2}$$

$$\text{and } g = \left[\frac{V}{R}\left(\frac{\partial P}{\partial T}\right)_V\right]^2 \quad . \tag{3}$$

R is the universal gas constant (8.314 $\mathrm{JK^{-1}\ mol^{-1}}$), M is the molar mass of the gas in kg, P is the pressure ($\mathrm{Nm^{-2}}$), V is the volume ($\mathrm{m^3}$) and C_V is the specific heat at constant volume ($\mathrm{JK^{-1}\ mol^{-1}}$).

Assuming an ideal gas equation of state for one mole of gas,

$$PV = RT \quad , \tag{4}$$

and taking partial derivatives, we arrive at the familiar expression

$$V_S = \left(\frac{\gamma RT}{M}\right)^{\frac{1}{2}} \tag{5}$$

where $\gamma = C_P/C_V$, and use has been made of the ideal gas identity

$$C_P = C_V + R.$$

The velocity of sound in an ideal gas is frequently expressed in terms of its pressure and density,

$$V_S = \left(\frac{\gamma P}{\rho}\right)^{\frac{1}{2}} \tag{6}$$

and indeed, gas densities at known temperature and pressure are frequently inferred from sound velocity measurements.

In this work, sound velocities have been measured at atmospheric pressure (1.01325×10^5 Nm^{-2}) in several possible CRID gases, over a temperature range between 25°C and 45°C. In addition, other reference gases have been studied, especially where previously tabulated sound velocity measurements are plentiful. Table II lists density, molecular weight and some specific heat data for the various gases considered in this work.

It will be seen (Fig. 6) that while for nitrogen there is good agreement ($\sim 0.3\%$) between the measured sound velocity and the ideal gas prediction of Eq. 5, significant divergences (Fig. 7-10) are seen for the other gases, varying between $\sim 0.5\%$ for methane and about 4% for C_5F_{12}. These divergences are due to the non-ideal nature of these gases, which require treatment with a more realistic equation of state.

Before considering some more sophisticated equations of state and comparing our sound velocity measurements with their predictions (Table III), it is worth commenting that a fit to sound velocity measurements offers a powerful aid to the determination of the equation of state of a gas (or gas mixture) particularly when use is made of a complex empirical formalism containing many free parameters. When known, the equation of state can be used to reveal, for example, the mixing ratio of a binary mixture from a single velocity measurement at known temperature–the main purpose of this work–or can reveal the temperature of a volume of gas of known composition. Such a "sonic thermometer" might find application in many forms of gaseous ionization detectors, where electrostatic constraints restrict the placing of electrical temperature sensors to the walls of the gas enclosure, inhibiting measurement within the gas volume.

The simplest approximation to the equation of state of a real gas is the Van der Waals

equation

$$\left(P + \frac{a}{V^2}\right)(V - b) = RT \tag{7}$$

where the term a is a measure of the attractive force between the molecules, and b is due to their finite volume and general incompressibility. For any pure gas, the Van der Waals constants a and b can be expressed in terms of the critical temperature and pressure, T_C and P_C, [11] as

$$a = \frac{27R^2T_C^2}{64P_C}, \qquad b = \frac{RT_C}{8P_C} \quad . \tag{8}$$

Applying Eqs. 1-3 to the Van der Waals (VDW) equation of state (Eq. 7), we arrive at an expression for V_S, to lowest order in a and b, in terms of standard tabulated parameters, *viz.*;

$$V_S = \left[\frac{RT}{M}\left(\frac{PV}{RT}\left(1 - \frac{a}{PV^2} + \frac{b}{V}\right) + \frac{R}{C_V}\left(1 + \frac{2b}{V}\right)\right)\right]^{\frac{1}{2}} \tag{9}$$

The term in the second bracket represents in some sense an effective ratio of specific heats for the Van der Waals gas, so that Eqs. 9 and 5 have the same fundamental form. Indeed, when $a = b = 0$ (the definition of an ideal gas) Eq. 9 reduces exactly to Eq. 5.

A number of complex, empirical equations of state have been developed to model the behavior of specific real gases or groups of real gases to very high accuracy. One such equation, suitable for light hydrocarbons, has been developed by Benedict, Webb and Rubin [12](BWR) was subsequently modified by Lee and Kesler [13], and is particularly suitable for three of the gases considered in this work.

In models of real gases, it is conventional to define a "compressibility factor" Z such that

$$Z \equiv \frac{PV}{RT} \tag{10}$$

where $Z = 1$ is the definition of an ideal gas. Compressibility data for many common gases are tabulated over a wide range of temperature and pressure in Ref. 9.

The modified BWR equation of state [13] may be written

$$Z(T_r, P_r) = \frac{P_r V_r}{T_r} \tag{11.1}$$

where

$$T_r = \frac{T}{T_C}, P_r = \frac{P}{P_C} \text{ and } V_r = \frac{P_C V}{R T_C}$$

T_r, P_r and V_r are the dimensionless "reduced" temperature, pressure and volume. The right hand side of Eq. 11.1 is expressed as an expansion in terms of a series of empirical constants

$$\begin{aligned} Z(T_r, P_r)_{BWR} &= 1 + \frac{B}{V_r} + \frac{C}{V_r^2} + \frac{D}{V_r^5} + \frac{C_4}{T_r^3 V_r^2}\left(\beta + 2\alpha V_r^2\right) \exp\left(-\frac{\alpha}{V_r^2}\right) \\ \text{where } B &= b_1 - \frac{b_2}{T_r} - \frac{b_3}{T_r^2} - \frac{b_4}{T_r^3} \\ C &= C_1 - \frac{C_2}{T_r} + \frac{C_3}{T_r^3} \\ \text{and } D &= d_1 + \frac{d_2}{T_r} \quad . \end{aligned} \tag{11.2}$$

The constants $b_1 \rightarrow b_4$, $C_1 \rightarrow C_4$, d_1 and d_2, α and β are tabulated in Ref. 13. In this work, the right hand side of Eq. 11.2 has been solved iteratively for each hydrocarbon gas to yield V_r in terms of P_r and T_r; these parameters having been evaluated at atmospheric pressure and temperatures ranging between 25°C and 45°C, respectively.

An equation of state of the form of Eq. 11 is said to be "generalized" since it is applicable, with the exception of empirical parameters specific to certain gases, to any gas whose critical temperature and pressure are known. Generalized equations of state are based on an assumption, known as the "principle of corresponding states," wherein all gases, measured at the same reduced temperature and pressure, deviate from ideal gas behavior to the same degree and have roughly equal compressibility factors [11]. This principle has found wide application in formulating equations of state and is reasonably accurate. Its precision has been further improved with the introduction of a third parameter or "acentric" factor, w.

At constant reduced temperature and pressure, the compressibility factor may be adequately represented by [14–16]

$$Z(T_r, P_r) = Z^{(o)} + wZ^{(1)} \tag{12}$$

where $Z^{(o)}$ is the compressibility factor for a simple gas (for example Argon or Krypton) and $Z^{(1)}$ is the deviation of the real gas from a simple gas approximation. $Z^{(o)}$ and $Z^{(1)}$ are extensively tabulated as functions of reduced temperature and pressure in Ref. 13 while w is tabulated for a variety of gases in Ref. 11.

Eqs. 10-12 fully define the three parameter correlation developed by Lee and Kesler and used in this work. It should be noted that while such correlations are generally highly accurate and widely applicable, even to gas mixtures (§4.3) they have been found to be inaccurate for highly polar gases, and for mixtures of gases which associate.

To facilitate sound velocity calculations using the BWR equation of state, we follow the convention of Whiting and Ackerberg [17] and recast Eq. 1 in the form

$$V_S = \left[\left(\frac{C_P}{C_V} \right) \left(\frac{ZRT}{M} \right) \left(1 - \frac{P_r}{Z} \left(\frac{\partial Z}{\partial P_r} \right)_{T_r} \right)^{-1} \right]^{\frac{1}{2}} \tag{13}$$

In Eq. 13, the thermodynamic parameters Z, C_P, C_V and $\left(\frac{\partial Z}{\partial P_r}\right)_{T_r}$ may be calculated for each gas from its critical temperature and pressure and its acentric factor (with expressions of the same form as Eq. 12) according to the correspondence phenomenology of Lee and Kesler, or may be found from published tabulations [13, 18–21]. In either case, the evaluation of Eq. 13 depends on tabulated values of C_P°, the ideal gas value of the constant pressure heat capacity —*i.e.*, the value of C_P in the limit $P \to 0$, $V \to \infty$ such that T remains constant. These values are extensively tabulated for a variety of gases in Refs. 18 and 21.

In Table III we compare our velocity measurements for single component gases with the theoretical predictions of the three different equations of state and tabulate the percentage deviation between each prediction and measurement. Figures 6–10 show the variation of the measured sound velocity with temperature for each gas, and compare them to the three theoretical predictions.

With the exception of C_5F_{12}, we observe, as expected, that the accuracy of the velocity predictions improves as the sophistication of the equation of state increases. The ideal gas assumption holds quite well for nitrogen and methane, but begins to break down when applied to isobutane (boiling point $-12°C$ at 1 Atmosphere), and is therefore even less appropriate for C_5F_{12}. The Van der Waals equation of state is quite accurate (within 1% of measurements) for nitrogen and the hydrocarbons, while the predictions of the BWR equation of state are very precise, lying within the estimated $\pm$ 0.3% systematic uncertainty in our velocity measurements (§3.3).

The source of error in the theoretical predictions—other than the limitations of the theories themselves—is the uncertainty present in tabulated thermodynamic data: $C_V(T)$ is needed for ideal gas and VDW predictions (Eqs. 5 and 9), while w and $C_P^\circ(T)$ data are required for the BWR analysis.

The larger divergences between our velocity measurements in C_5F_{12} and the various models come as no surprise, since few of the C_5F_{12} thermodynamic parameters are presently well known, due to the very limited world manufacture and use of this material. The BWR velocity predictions have relied on "educated guesses" for the C_5F_{12} acentric factor w and C_P° (Table IV) based on those of n-pentane, the hydrocarbon with the most similar molecular structure. Since this choice has no real theoretical justification, we have varied w over a wide range (up to a factor of 4), taking in the values for some of the other fluorocarbons, including Freon-12 (CCl_2F_2 : $w = 0.158$), Freon-113 ($C_2Cl_3F_3$: $w = 0.249$) and Freon-11 (CCl_3F: $w = 0.295$). These changes however, taken with or without a similar variation in C_P°, altered the BWR velocity predictions by less than 1%. This is not surprising however, since no attempt was made to adjust the parameters of the BWR equation (Eq. 11.2)—specific to light hydrocarbons—to fit our data.

Under the assumption that the value of the ratio of specific heats of a gas is independent of temperature, the variation of sound velocity with temperature is given by

$$V_{s(T_1)} = V_{s(T_0)}\sqrt{\frac{T_1}{T_0}}$$

where T_0 and T_1 are absolute temperatures. Generally however, as we shall see, precise pre-

dictions of the velocity of sound in gases require that account be taken of the temperature dependence of their specific heats.

The values of thermodynamic constants used in this work are displayed in Table IV. In all cases, C_V, C_P° or γ are assumed to vary linearly with temperature, for example

$$C_P^\circ(T) = C_P^\circ(T_\circ) + \frac{dC_P^\circ}{dT}(T - T_\circ) \tag{14}$$

where we choose $T_\circ = 25°\mathrm{C}$.

This linear assumption is reasonably accurate over our narrow temperature range. The temperature gradients $\left(\frac{d\gamma}{dT}, \frac{dC_P^\circ}{dT}\right)$ of Table IV are based on linear interpolations of available reference data [9, 10, 19, 21, 22], and are, particularly in the case of γ, subject to error due to scarcity of data. This error is manifested in the slightly different gradients of the theoretical and measured sound velocity temperature dependencies, which would be equal if $\gamma(T)$ were correctly interpolated. Nevertheless the good average agreement between the predicted and measured velocities leads us to conclude that our estimates are reliable.

4.2 The Velocity of Sound in Binary Gas Mixtures

Although, as we have seen, the speed of sound in single-component gases is well understood theoretically, accurate predictions of sound velocity in gas mixtures prove less tractable theoretically due to problems which arise in the definition of parameters to represent the average physical properties of the mixture. There are further difficulties in the formulation of empirical expressions to accurately describe these average properties for a wide variety of mixtures of different gases.

In our first and simplest approximation, the velocity of sound in a gas mixture, V_m, is assumed to be linearly proportional to the concentration *by weight* of the components

$$V_m = \frac{\sum_i X_i \rho_i V_i}{\sum_i X_i \rho_i} \tag{15}$$

where X_i is the molar concentration of the *ith* component, ρ_i is its density at the measurement temperature, and V_i is the measured velocity in the pure *ith* component gas. This "linear

density weight" formula has the advantage of simplicity and freedom from dependence on tabulated thermodynamic data. The formula is accurate ($\sim$ 0.1%) for sufficiently ideal gas mixtures, for example air (considering the three principal components N_2, O_2 and Ar), and neon-helium (Figs. 11 and 12), but is much less accurate (error of 1-3%) in predicting the velocities in the non-ideal hydrocarbon mixtures with CRID applications. It is of course possible to construct an empirical mixture velocity formula from theoretical considerations; the simplest approach uses the ideal gas expression (Eq. 6) to assert that

$$\left(\frac{\rho}{\gamma}\right)^{\frac{1}{2}} V_S = \sqrt{P} \ , \text{ a constant.}$$

Thus, for any component, i, we may write

$$V_m = \left[\frac{\rho_i \gamma_m}{\rho_m \gamma_i}\right]^{\frac{1}{2}} V_i \tag{16}$$

$$\text{where } \rho_m = \sum_i X_i \rho_i$$

The difficulty of this approach lies in the determination of γ_m. The correct procedure for an ideal gas is to weight the individual heat capacities by mass fraction [24]. If W_i is the mass fraction of the *ith* component of the mixture, then

$$\gamma_m = \frac{C_{P_m}}{C_{V_m}} = \frac{\sum_i W_i C_{P_i}}{\sum_i W_i C_{V_i}} \tag{17}$$

Unfortunately, Eq. 17 requires use of tabulated heat capacity data, together with their inherent uncertainties. Some of these however can be eliminated by making use of the fact that

$$\gamma_m = 1 + \frac{R}{C_{p_m} - R}$$

We have found– despite its dependence on tabulated heat capacity data– that the ideal gas formalism of Eqs. 16 and 17 leads to reasonably accurate predictions (typical error of $\sim$ 1% - Table V) for the sound velocity in the various CRID hydrocarbon mixtures.

Our results for pure gases suggest that more accurate velocity predictions can be achieved with the use of realistic gas equations of state. We have seen that the sound velocity in a pure gas can be predicted from its critical temperature and pressure, under both the VDW or BWR equations of state. Under their three-parameter correlation scheme, Lee and Kesler [13] have developed a set of empirical mixing rules to determine a "pseudocritical" temperature and pressure and "pseudoacentric" factor for mixtures of light hydrocarbons.

The critical volume, V_{Ci}, of the *ith* component is given by

$$V_{C_i} = Z_{C_i} R T_{C_i} / P_{C_i} \quad , \tag{18}$$

$$\text{where } Z_{C_i} = 0.2905 - 0.085 w_i \tag{19}$$

The first numeric factor in Eq. 19 represents the compressibility factor of an ideal gas at its critical point, while the second is the average empirical compressibility deviation for the light hydrocarbons.

The pseudo-critical volume of the gas mixture, V_{C_m}, is given by a molar concentration–weighted summation over all component combinations:

$$V_{C_m} = \frac{1}{8} \sum_{i=1}^{n} \sum_{j=1}^{n} X_i X_j \left(V_{C_i}^{1/3} + V_{C_j}^{1/3} \right)^3 \tag{20}$$

while the three correlation parameters are defined by

$$\begin{aligned} T_{C_m} &= \frac{1}{8 V_{C_m}} \sum_{i=1}^{n} \sum_{j=1}^{n} X_i X_j \left(V_{C_i}^{1/3} + V_{C_j}^{1/3} \right)^3 \left(T_{C_i} T_{C_j} \right)^{1/2} \\ w_m &= \sum_{i=1}^{n} X_i w_i \\ P_{C_m} &= (0.2905 - 0.085 w_m) R T_{C_m} / V_{C_m} \end{aligned} \tag{21}$$

The pseudocritical temperature and pressure can be applied to the BWR equation of state (Eq. 11), and to the Van der Waals equation (Eq. 7) using Eq. 8. The Van der Waals formalism

depends on C_V tabulations for real gases (Eq. 9), while the BWR predictions rely only on ideal gas heat capacity data (Eq. 13). For each component, C_{V_i} is temperature–corrected as in Eq. 14 and formed into a mass–weighted average for the mixture, as in the denominator of Eq. 17.

Velocity predictions for the three equations of state are compared, as a function of gas mixture composition, with the experimentally measured velocities in Figs. 13–16. The average percentage deviations between the predictions and experimental measurements are shown in Table V. It is evident that the Lee and Kesler pseudocritical mixture rules (Eqs. 17 and 21) are no more accurate than the ideal gas mixing formula (Eqs. 16, 17), but it should be remembered that the latter is more tightly constrained, making use of sound velocity data (Eq. 16).

We also notice that once the Lee and Kesler mixing rules are adopted, the choice of equation of state (VDW or BWR) makes little difference to the accuracy of the final results: the limitation is ultimately set by the mixing rules themselves. Since these rules were developed as an average for light hydrocarbons we do not expect them to be very accurate for mixtures containing non-hydrocarbons such as N_2/C_4H_{10}, and in particular N_2/C_5F_{12}. Conversely, the prediction for the most likely choice of CRID TPC drift gas, CH_4/C_2H_6, is extremely good, while that for CH_4/C_4H_{10} is also reasonably accurate.

We observe, as expected, large differences between our velocity measurements and the predictions for N_2/C_5F_{12} mixtures. These could presumably be reduced by the adjustment of the numeric factors of the BWR equation (Eq. 11.2) and the Lee and Kesler mixing formulae (Eq. 19, 21). It seems unlikely however that the formalism can be extended to accommodate all the gases of CRID interest with high accuracy, and indeed this is outside the scope of the present work.

Table V summarizes the predictive power of the existing equations of state. For mixtures containing hydrocarbons, percentage range determinations of the binary mixture ratio can be made from a single velocity measurement at known temperature, using either the density weighting formula (N_2/C_4H_{10}) or one of the three equations of state (CH_4/C_2H_6, CH_4/C_4H_{10}). The predictions of the various equations of state are most easily represented in the form of look-up tables of velocity *vs* concentration, which are generated from numerical fits to the

predicted curves. With fine enough ($\sim$ 1%) binning, the concentration corresponding to a particular velocity measurement made with the CAMAC scaler apparatus of §3.1 can be found by simple interpolation, with an uncertainty given by

$$\Delta X = \frac{\Delta V}{m} \tag{22}$$

where ΔV is the systematic velocity measurement error and m is the gradient of the velocity-concentration curve interpolated across the bin spanning the velocity measurement. Since it would be rather wasteful to fit the velocity-concentration curves on line to generate the look-up tables, velocity-concentration data will probably be stored at a few temperatures to allow the table corresponding to the measurement temperature to be found by a linear temperature interpolation. In this way, it should be possible—for the three mixtures containing hydrocarbons—to make $\sim$ 1% mixture determinations using a single sound velocity measurement in conjunction with existing mixing rules and equations of state.

It is obvious however that none of the theoretical models is well suited to a N_2/C_5F_{12} mixture. Accurate determinations of these mixtures are only possible from a numerical fit to an experimentally-measured velocity-composition curve (§4.3).

4.3 The Fitted Velocity–Concentration Curves

High precision concentration determinations in any binary gas mixture may be achieved, independent of any knowledge of the equation of state, from a numerical fit to sound velocity measurements taken at known temperature and various known compositions. As in §4.2, the fit can generate a precalibrated look up table of velocity *vs* concentration which can be used to reveal the gas mixture.

The velocity-concentration curves for all the mixtures considered in this work have been fitted, using the MINUIT program[25] to a simple polynomial of the form

$$[V(X)]_T = A + BX + CX^2 + DX^3 + \ldots$$

where A represents the sound velocity in the pure carrier gas (CH_4 or N_2) and X is the percentage concentration of the additive (C_2H_6, C_4H_{10} or C_5F_{12}).

The results of the fits are summarized in Table VI. We have found that a cubic parametrization is the minimum needed to satisfactorily fit ($0.5 \leq \chi^2/DF \leq 1.5$) the experimental data for CH_4/C_2H_6 and N_2/C_4H_{10}. In mixtures where the difference in velocity between the pure components is greater: CH_4/C_4H_{10} (451/213) and N_2/C_5F_{12} (355/94: with fit shown in Fig. 16), the steeper velocity-concentration curves require a quartic fit.

Whatever the chosen function, the mixture concentration and its uncertainty are easily obtained by interpolation from look-up tables stored at a number of reference temperatures. In this way a single velocity measurement at known temperature can reveal the gas mixture, just as it can when the equation of state is known.

In this work, each velocity-concentration curve has been fitted using an iterative two-step procedure. At first, the experimental velocity measurements were assigned a nominal 1% error, and the local gradients from a preliminary fit used (via. Eq. 22) to project the systematic mixture uncertainty onto the velocity axis for combination with its 0.3% systematic error. The data were then refitted with these errors to produce the parameterization of Table VI.

In the present work, the uncertainty in the *absolute* determination of binary mixtures is limited to $\sim \pm 1\%$ by the systematic uncertainties in the calibration mixtures. In the future, look-up tables will be generated at a variety of temperatures using calibration mixtures set up to an accuracy of better than $\pm$ 0.5% either by partial volume or partial pressure mixing, depending on the nature of the binary mixtures to be monitored.

The use of a high sensitivity readout amplifier affords excellent reproducibility in our velocity measurements. The sonar electronics is triggered once per second, and under stable temperature conditions the count rate from the CAMAC scaler is stable to within five counts; this represents a 0.06% velocity uncertainty in CH_4, the fastest of the gases. The instrument is therefore very sensitive to changes in temperature or gas composition, and can act as an early warning of the malfunction of a mass flow controller in the TPC gas supply circuit.

As an example of the precision (at constant temperature) with which binary mixture *stability* might be monitored. Table VII has been generated by applying a 0.1% sound velocity resolution error to Eq. 22. We see as expected that the precision is greatest in the steepest regions of the curves, and that greater sensitivity is available in those mixtures whose steeper

curves require a quartic parameterization.

In normal CRID operation, we expect to use a drift gas mixture of 80% CH_4/20% C_2H_6, in which stability fluctuations of $\sim$ 0.2% should be detectable. In the radiator system, 0.1% fluctuations should be detectable over the whole range of compositions encountered during C_5F_{12} filling and recovery.

5. Summary and Conclusions

We have seen how a simple sonar device can be used in an on-line mode to reveal the composition or monitor the stability of a binary gas mixture from sound velocity measurements at known temperature.

For a number of mixtures containing hydrocarbons, compositions can be deduced solely from theoretical considerations, while more "exotic" gas mixtures can be analysed with the aid of precalibrated velocity tables.

The sonar system can be completely automated–including the provision of computer-operated gas selection valves–and promises to be useful for the routine monitoring of binary gas mixtures found in many drift chamber applications.

Acknowledgement

One of us (G. Crawford) is grateful to Prof. D.W.G.S. Leith and the members of SLAC Group B for their hospitality during the summer of 1986.

REFERENCES

[1] S. Williams et al., IEEE Trans. Nucl. Sci. NS-32, 681 (1985).

[2] S. Williams et al., "Cerenkov Ring Imaging Detector Development at SLAC," SLAC-PUB-3360 (1984).

[3] V. Ashford et al., IEEE Trans. Nucl. Sci. NS-33, 113 (1986)

[4] See for example M. Breidenbach, IEEE, Trans. Nucl. Sci. NS-33, 46, (1986).

[5] D. Anderson, IEEE Trans. Nucl. Sci. NS28, 842 (1981).

[6] Polaroid Corp., Ultrasonic Ranging System User's Manual and Application Notes. Polaroid Corporation, Commercial/ Battery Division, 575 Technology Square 3, Cambridge, MA 02139.

[7] R. L. Abbey and G. E. Barlow, Austral. J. Sci. Res. Ser. A., Vol. 1, No. 2, 175 (1948).

[8] See for example American Institute of Physics Handbook, 3rd Edition, McGraw Hill (1972). Ed. L. L. Beranek, p 3-73.

[9] Matheson Gas Data Book, 6th Edition (1980) Ed. W. Braker & A. Mossman.

[10] Thermodynamic tables for "Flutec PP50" perfluoro-n-pentane. (unpublished) supplied by I.S.C. Chemicals Ltd. Avonmonth, Bristol BS11 GHP, U.K.

[11] J. M. Smith and H. C. Van Ness "Introduction to Chemical Engineering Thermodynamics," 3rd Edition McGraw Hill (1975).

[12] M. Benedict, G. B. Webb and L. C. Rubin, Journ. Chem. Phys. 8, 334 (1940).

[13] B. I. Lee and M. G Kesler, AICHE Journal, Vol. 21, No. 3, 510 (1975).

[14] K. S. Pitzer, D. Z. Lippman,, R. F. Curl, Jr., C. M Huggins and D.E. Peterson, J. Am. Chem. Soc. 77, 3433 (1955).

[15] K. S. Pitzer and R. F. Curl, Jr., J. Am. Chem. Soc. 79, 2369 (1957).

[16] K. S. Pitzer and R. F. Curl, Jr., Ind. Eng. Chem. 50, 265 (1958).

[17] W. B. Whiting II and R. C. Ackerberg, A. I. Ch. E. Journal, Vol 24, No. 2, 341 (1978).

[18] F. D. Rossini et al., "Selected Values of Physical and Thermodynamic Properties of Hydrocarbons and Related Compounds," American Petroleum Institute Research Project 44 (1952).

[19] B. D. Smith and R. Srivastava, "Thermodynamic Data for Pure Compounds; Part A; Hydrocarbons and Ketones," Elsevier (1986).

[20] W. B. Whiting and R. C. Ackerberg, Document No. 03194, National Auxiliary Publications Service, c/o Burrows Microfilm Systems, 248 Hempstead Turnpike, West Hempstead, NY 11552, U.S.A.
This document contains tabulations of $\left(\frac{\partial Z^{(\circ)}}{\partial P_r}\right)_{T_r}$ and $\left(\frac{\partial Z^{(1)}}{\partial P_r}\right)_{T_r}$ not included in Ref. 17.

[21] K. M. Marsh *et al.*, TRC Thermodynamic Tables-Hydrocarbons, Thermodynamics Research Center, Texas A&M Univ. (1986).

[22] International Critical Tables of numerical data, physics, chemistry and technology, Mc. Graw Hill, New York (1933) Ed. E. Washburn.

[23] Handbook of Chemistry and Physics, 65th Edition, CRC Press, Boca Raton, Florida (1985) Ed. R. Weast.

[24] See for example W. Geidt, "Thermophysics," Van Nostrand Reinhold (1971), p 316.

[25] MINUIT, CERN Computer Center Write-Up, D506, F. James and M. Roos, CERN Program Library (1977).

Table I. Systematic errors assumed in this work.

Property	Systematic Error
Gas Temperature	±0.3°C
Sound Velocity Measurement	±0.3%
Composition (MFC Mixtures)	±1.0%
Composition C_5F_{12}/N_2	±1.0%

Table II. Density, molecular weight and specific heat data for relevant gases: (after Refs. 9 and 10*)

GAS	Density (kg m^{-3}) (1 Atm, at T K)		Molecular Weight (kg)	Specific Heats, (J $mol^{-1}K^{-1}$) and Ratio (1 Atm, at T′ K)			
	ρ	T		C_P	C_V	γ	T′
Argon	1.784	273	0.036	20.83	12.48	1.669	300
Ethane	1.242	298	0.030	53.346	44.769	1.192	300
Helium	0.179	273	0.004	20.967	12.863	1.630	273
Isobutane	2.487	293	0.058	94.163	85.854	1.097	288.6
Methane	0.717	273	0.016	35.941	27.531	1.305	300
Neon	0.825	298	0.020	20.786	12.659	1.642	298
Nitrogen	1.146	298	0.028	28.980	20.600	1.407	300
Oxygen	1.309	298	0.032	29.427	20.817	1.414	298
Perfluoro-n-pentane (C_5F_{12})*	11.391	313	0.276	260.47 ± 3.06	260.31 ± 3.16	1.001 ± 0.017	303-323

Table III. Comparison of theory with experiment:
sound velocity in single component gases

Gas	Temp. (^{o}C)	Measured Velocity (ms^{-1})	Theoretical Predictions (% discrepancies)		
			Ideal Gas	Van der Waals	BWR
N_2	30	355.0	355.8 (0.2)	355.8 (0.2)	355.0 (0.0)
CH_4	30	451.0	453.2 (0.5)	452.4 (0.3)	452.0 (0.2)
C_2H_6	30	313.7	317.2 (1.1)	314.2 (0.2)	313.6 (0.03)
C_4H_{10}	30	213.1	218.4 (2.5)	214.5 (0.7)	212.8 (0.1)
C_5F_{12}	41	93.9	97.4 (3.7)	96.9 (3.2)	97.8 (4.2)

Table IV

Thermodynamic Data for Gases Used in This Work

Note: All values are at T = 25°C unless otherwise noted

Property	Gas N_2	CH_4	C_2H_6	C_4H_{10}	C_5F_{12}
Density[1] (kg m^{-3}), ρ	1.146	0.657	1.242	2.445	11.391[7†]
Critical Temperature[1](K), T_c	126.26	191.05	305.50	408.13	421.9[7]
Critical Pressure [1] (kPa), P_c	3400	4640	4914	3650	2048[7]
Molar Mass[1] [Kg], M	0.028	0.016	0.030	0.058	0.276[7]
Acentric Factor,[2] w	0.04[2]	0.011[3]	0.099[3]	0.184[3]	0.251[2] ††
Ratio of Specific Heats[1], $\frac{C_P}{C_V} = \gamma$	1.407*	1.305*	1.192*	1.097**	1.001[7†]
Rate of Change of γ with Temperature[4], $(°C^{-1})$ $\frac{d\gamma}{dT}$	0.0	5.33×10^{-4}	6.0×10^{-4}	2.67×10^{-4}	0.0[7]
Ideal Gas Heat Capacity at Constant Pressure[5] (JK^{-1} mol^{-1}), C_P°	29.125	35.69	52.47	96.65	120.83††
Rate of Change of C_P° with Temperature[6] ($J\ K^{-2}$ mol^{-1}) $\frac{dC_P^\circ}{dT}$	1.27×10^{-3}	3.43×10^{-2}	0.119	0.248	0.377††

Reference and Notes:

[1] Ref. (9)
[2] Ref. (11)
[3] Ref. (19)
[4] Values interpolated from available data (Ref. 22-23, see text)
[5] Ref. (21)
[6] Linear interpolation of data in Ref. (21)
[7] Ref. (10)

* data at T= 26.85 °C
** data at T = 15.6 °C
† data at T = 40.0 °C
†† estimates: see §4.3

Table V. Sound Velocity in Binary Gas Mixtures:

Percentage deviation between measurements and theory, averaged over range of concentration

Gas Mixture	Temp (°C)	Theoretical Predictions			
		Eq. 15	Eqs. 16, 17	Eqs. 17-21	Mixing Rule Eqs. 17-21
Equation of State		—	Ideal Gas	Van der Waals	BWR
CH_4/C_2H_6	30	0.86	0.31	0.34	0.47
CH_4/C_4H_{10}	30	2.45	1.30	1.01	1.04
N_2/C_4H_{10}	30	0.84	1.21	1.67	1.74
N_2/C_5F_{12}	41	18.9	13.2	14.5	11.9

Table VI. Fit Parameters for the Velocity-Concentration Curves.

Gas Mixture	Temp. (^{0}C)	Fit Value (Error) A	B	C	D	E
CH_4/C_2H_6	30	450.84 (1.2473)	-2.3186 (0.1106)	1.2789×10^{-2} (2.6025×10^{-3})	-3.3146×10^{-5} (1.6584×10^{-5})	–
CH_4/C_4H_{10}	30	450.98 (1.3125)	-7.1767 (0.2067)	0.1164 (9.6269×10^{-2})	-1.1073×10^{-3} (1.5336×10^{-4})	4.2350×10^{-6} (7.6814×10^{-7})
N_2/C_4H_{10}	30	354.13 (0.9938)	–3.0277 (9.0507×10^{-2})	2.6561×10^{-2} $2.1557\times10^{-3})$	-1.0395×10^{-4} (1.3728×10^{-5})	—
N_2/C_5F_{12}	41	360.85 (1.0561)	–10.112 (0.2047)	0.1875 (9.4186×10^{-3})	-1.7406×10^{-3} (1.4433×10^{-4})	6.1841×10^{-6} (7.0086×10^{-7})

Table VII Percentage resolution of gas mixture stability, as a function of composition*

Gas Mixture	CH_4/C_2H_6	CH_4/C_4H_{10}	N_2/C_4H_{10}	N_2/C_5F_{12}
Additive Concentration (%)				
10	0.2	0.1	0.1	< 0.1
20	0.2	0.1	0.1	< 0.1
30	0.2	0.1	0.2	< 0.1
40	0.3	0.1	0.2	< 0.1
50	0.3	0.2	0.2	0.1
60	0.3	0.2	0.3	0.1
70	0.3	0.2	0.3	0.1
80	0.4	0.2	0.3	0.1
90	0.4	0.3	0.3	0.1

---

* Example assumes constant temperature, with a 0.1% sound velocity measurement error — see text.

TABLE OF FIGURES

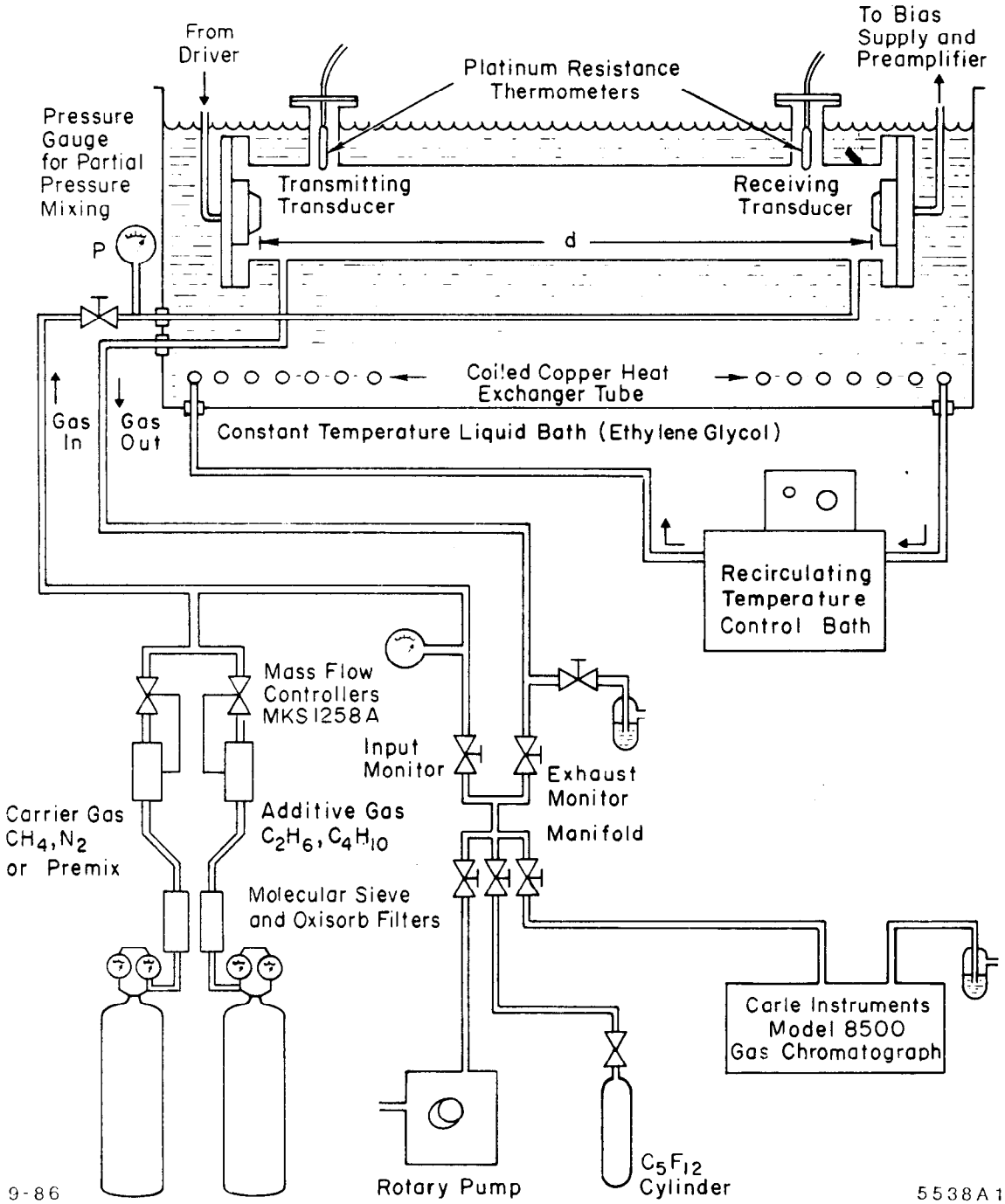
From Driver
To Bias Supply and Preamplifier
Platinum Resistance Thermometers
Pressure Gauge for Partial Pressure Mixing
Transmitting Transducer
Receiving Transducer
P
d
Coiled Copper Heat Exchanger Tube
Gas In
Gas Out
Constant Temperature Liquid Bath (Ethylene Glycol)
Recirculating Temperature Control Bath
Mass Flow Controllers MKS1258A
Input Monitor
Exhaust Monitor
Manifold
Carrier Gas CH_4, N_2 or Premix
Additive Gas C_2H_6, C_4H_{10}
Molecular Sieve and Oxisorb Filters
Carle Instruments Model 8500 Gas Chromatograph
Rotary Pump
C_5F_{12} Cylinder
9-86
5538A1

Fig. 1

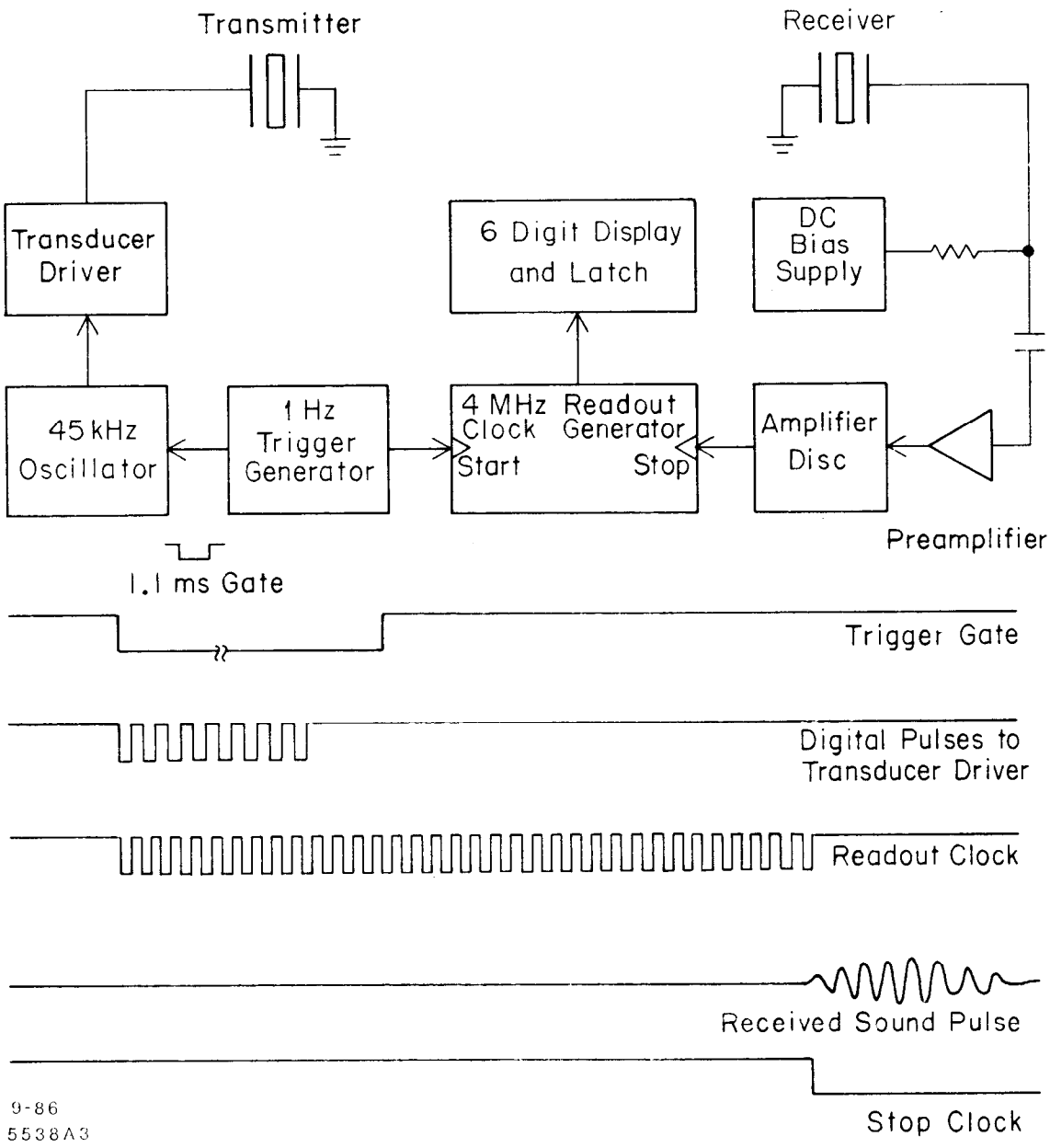
Transmitter
Receiver
Transducer Driver
6 Digit Display and Latch
DC Bias Supply
45 kHz Oscillator
1 Hz Trigger Generator
4 MHz Readout Clock Generator
Start
Stop
Amplifier Disc
Preamplifier
1.1 ms Gate
Trigger Gate
Digital Pulses to Transducer Driver
Readout Clock
Received Sound Pulse
Stop Clock
9-86
5538A3

Fig. 2

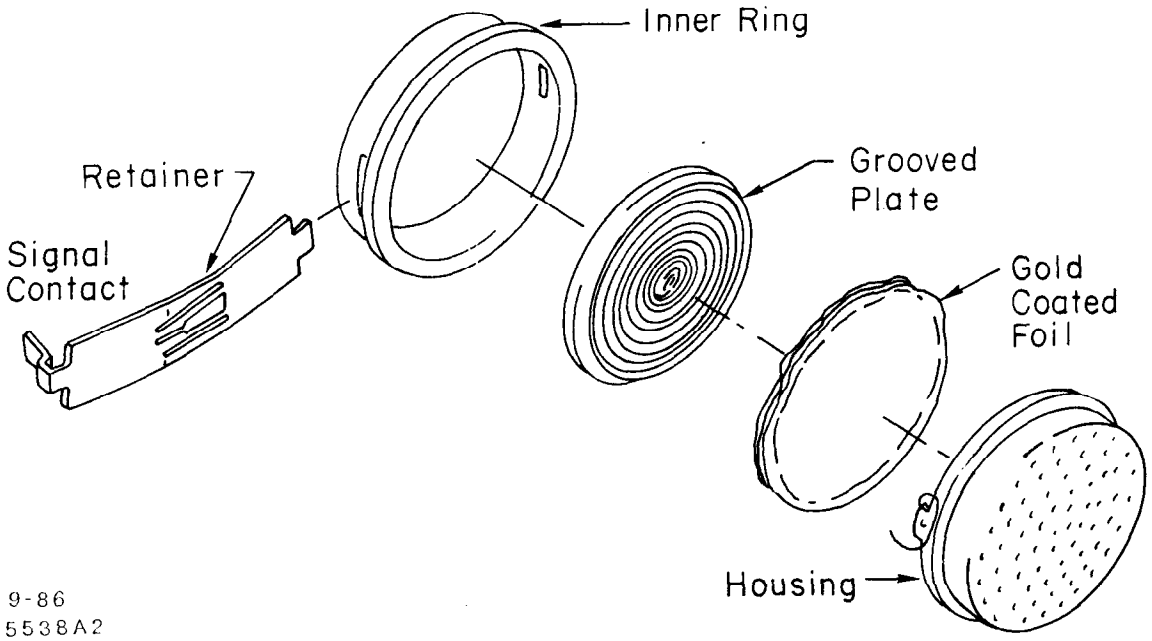
Inner Ring
Retainer
Grooved
Plate
Signal
Contact
Gold
Coated
Foil
Housing
9-86
5538A2

Fig. 3

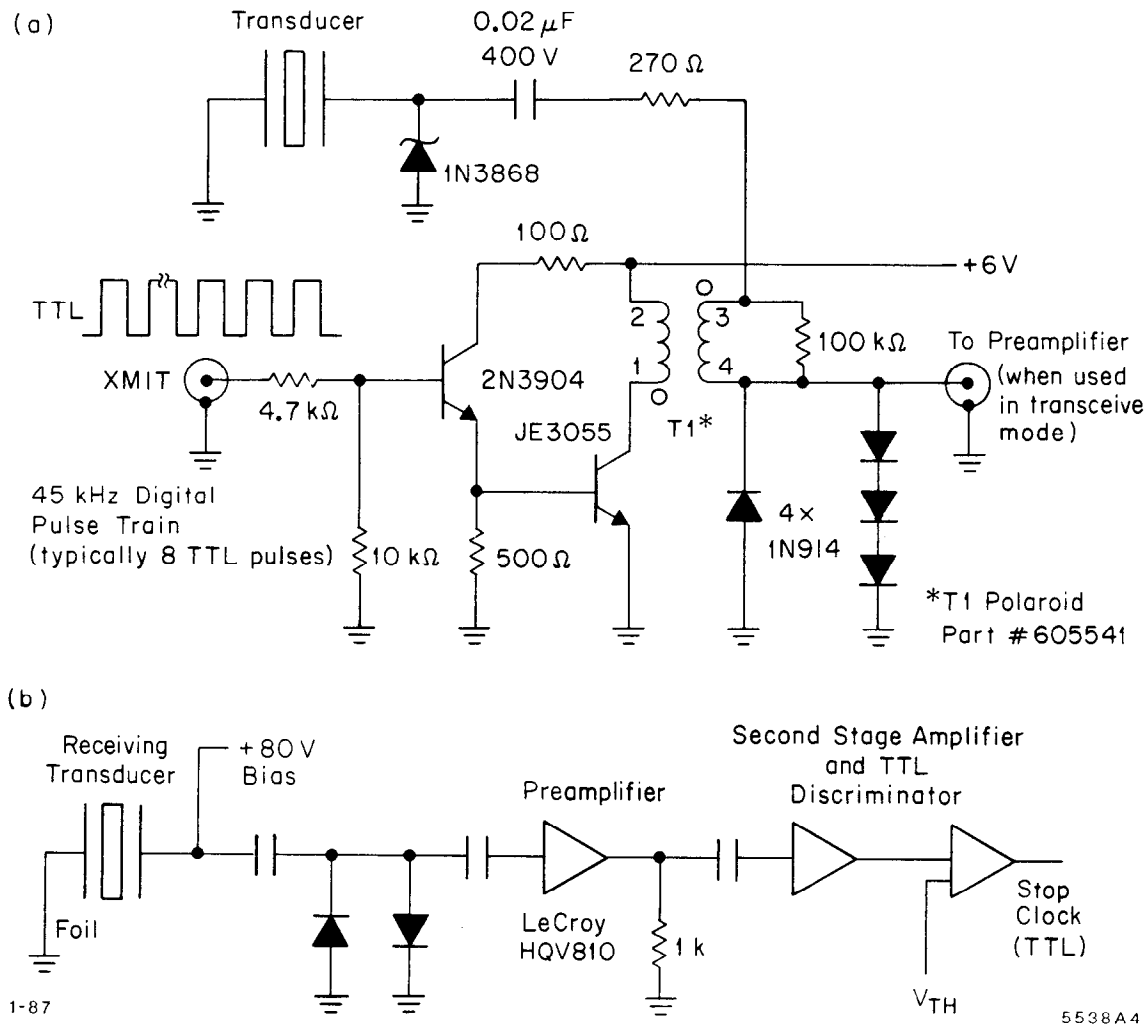
(a)
Transducer
0.02 μF
400 V
270 Ω
1N3868
100 Ω
+6V
TTL
XMIT
4.7 kΩ
2N3904
JE3055
T1*
100 kΩ
To Preamplifier
(when used
in transceive
mode)
45 kHz Digital
Pulse Train
(typically 8 TTL pulses)
10 kΩ
500 Ω
4×
1N914
*T1 Polaroid
Part #605541
(b)
Receiving
Transducer
+80 V
Bias
Preamplifier
Second Stage Amplifier
and TTL
Discriminator
Foil
LeCroy
HQV810
1 k
Stop
Clock
(TTL)
V_{TH}
1-87
5538A4

Fig. 4

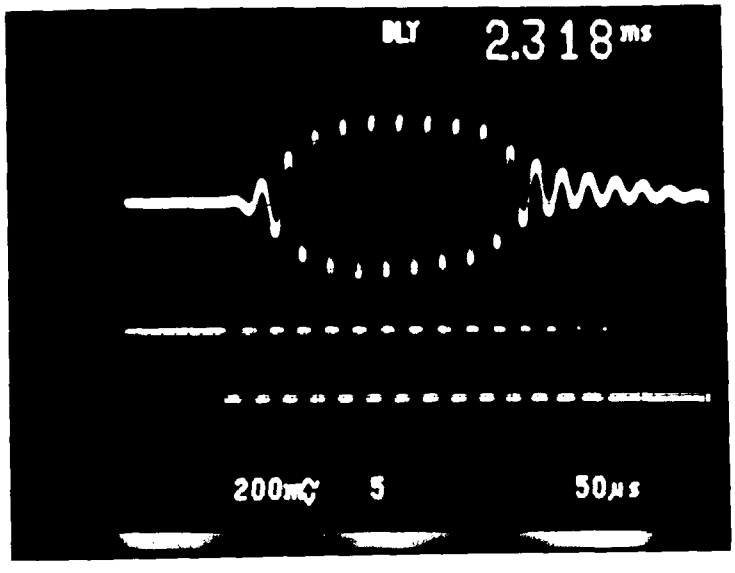

11-86 5538A6

Fig. 5

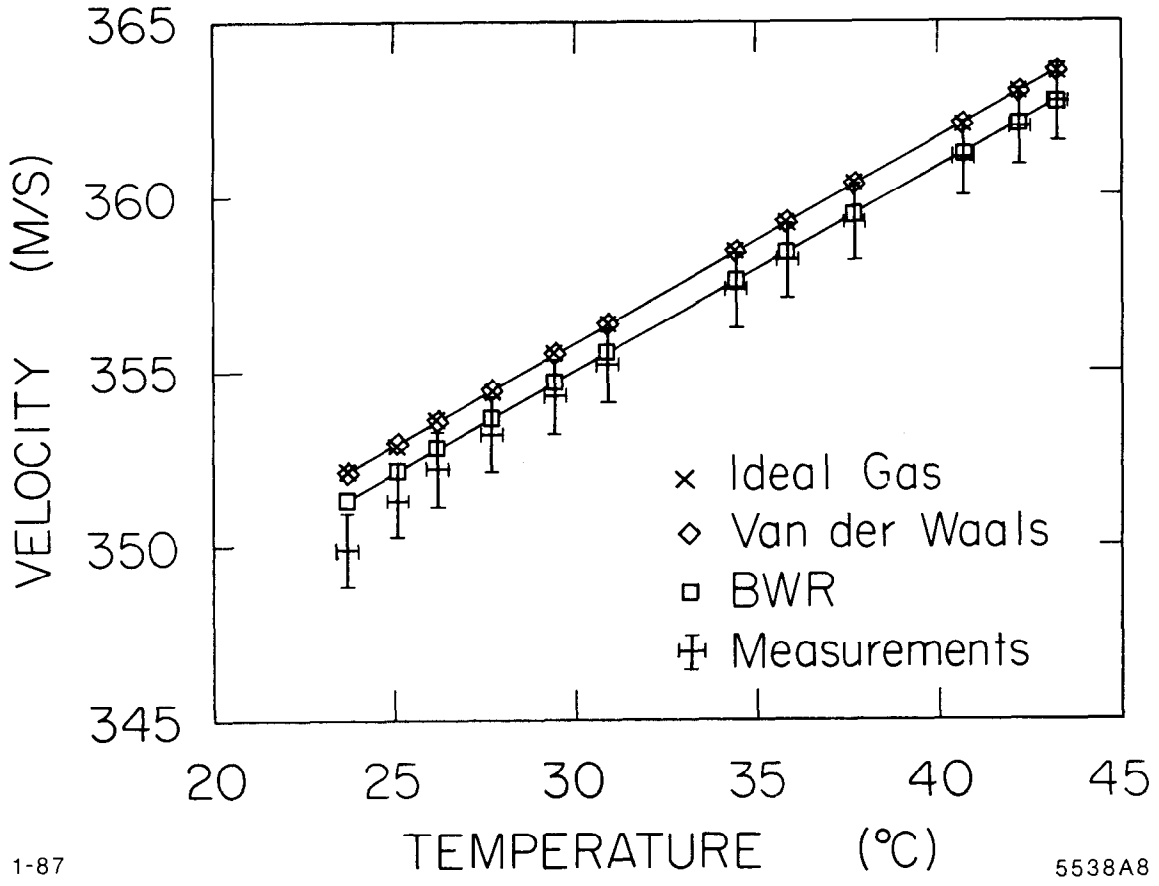
365
360
355
350
345
VELOCITY (M/S)
20
25
30
35
40
45
TEMPERATURE (°C)
× Ideal Gas
◇ Van der Waals
□ BWR
Measurements
1-87
5538A8

Fig. 6

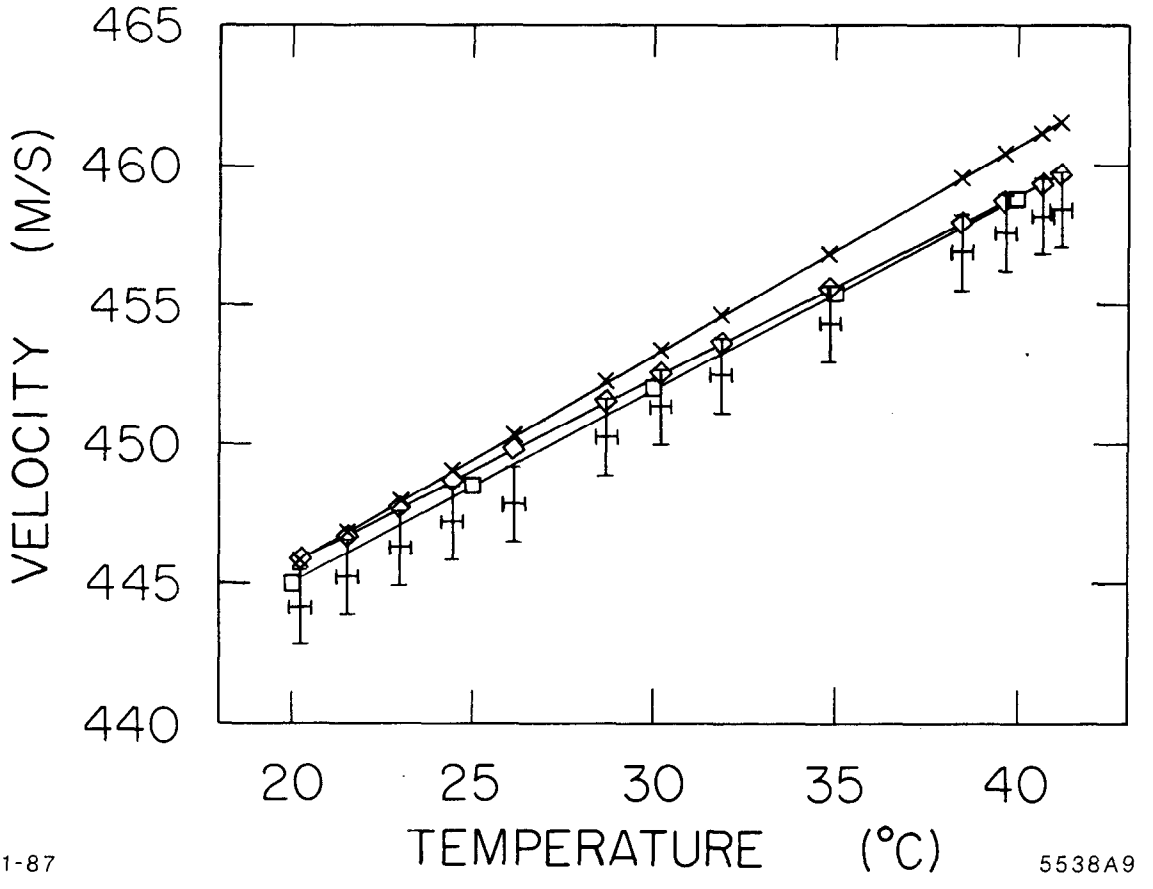
465
460
455
450
445
440
VELOCITY (M/S)
20
25
30
35
40
TEMPERATURE (°C)
1-87
5538A9

Fig. 7

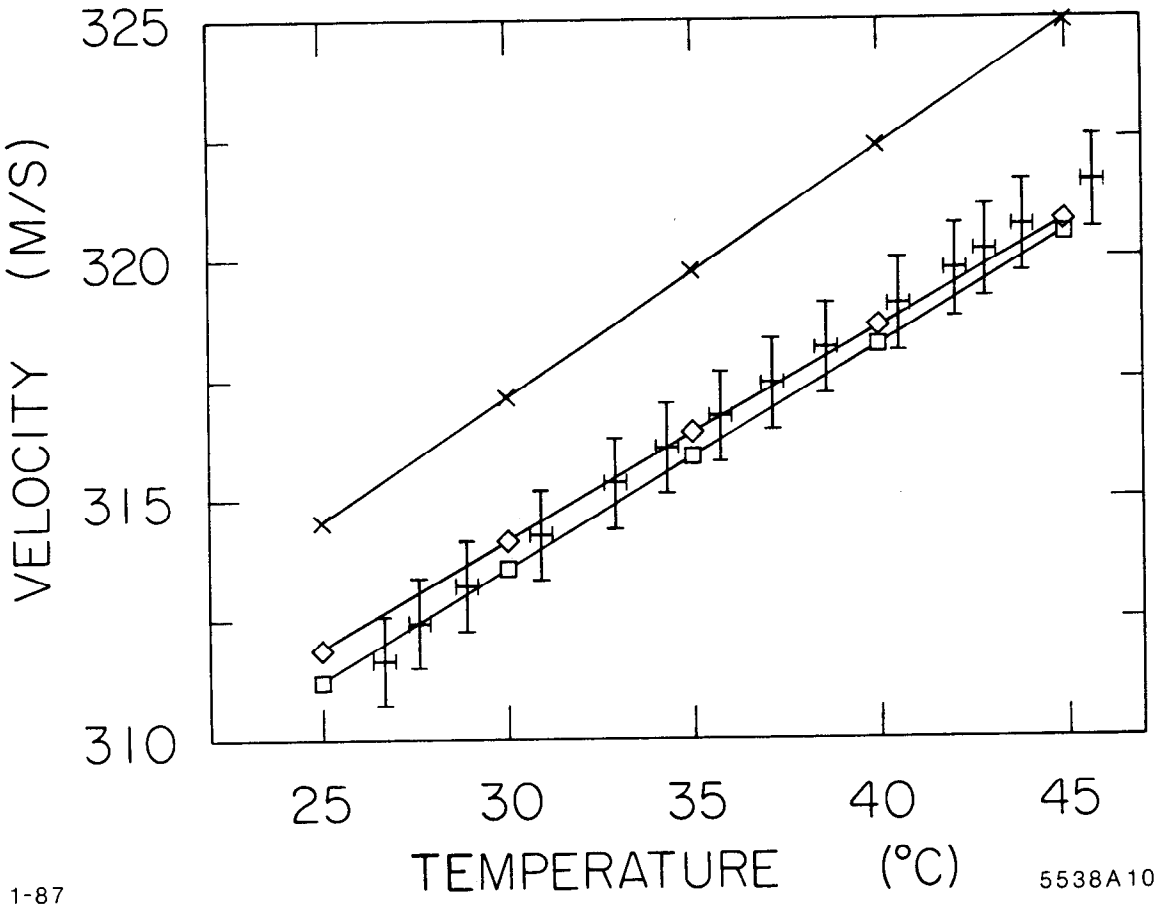
325
320
315
310
VELOCITY (M/S)
25
30
35
40
45
TEMPERATURE (°C)
1-87
5538A10

Fig. 8

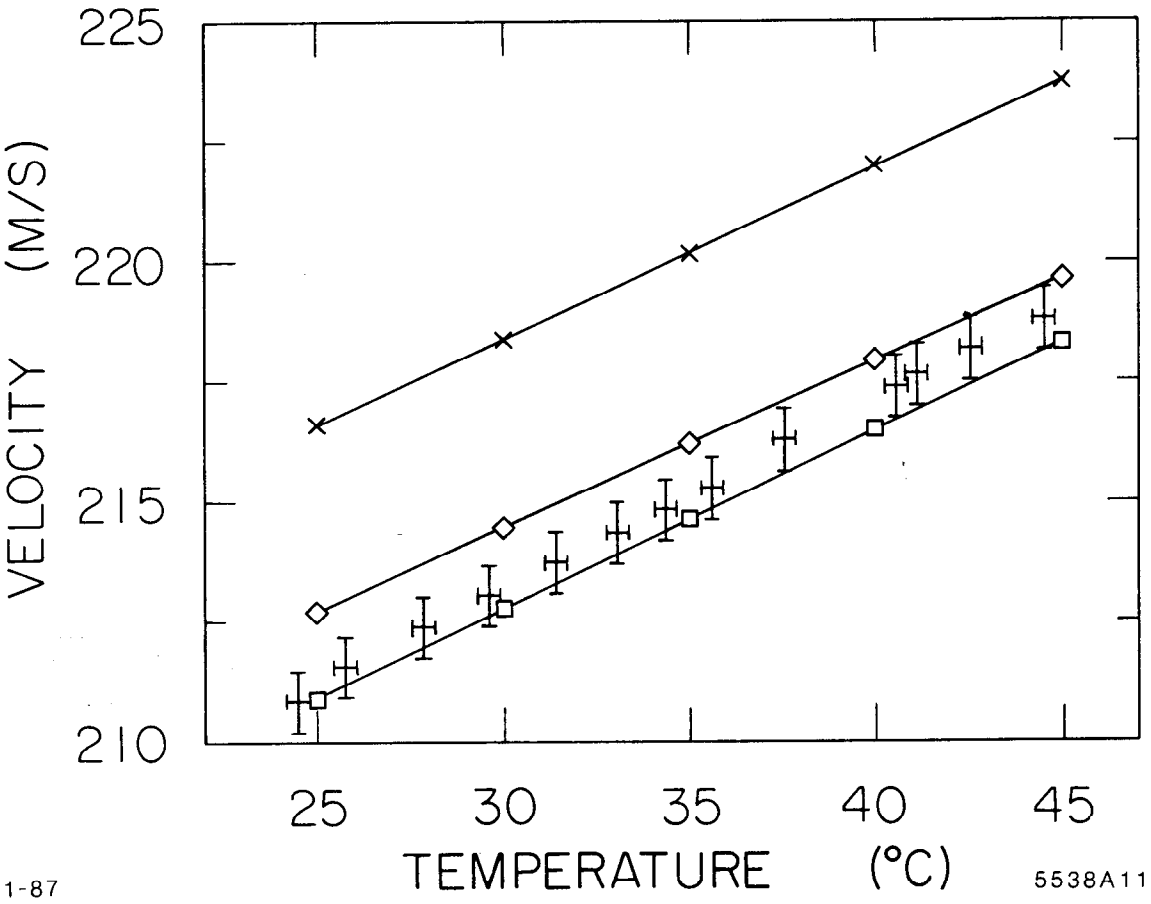
225
220
215
210
VELOCITY (M/S)
25
30
35
40
45
TEMPERATURE (°C)
1-87
5538A11

Fig. 9

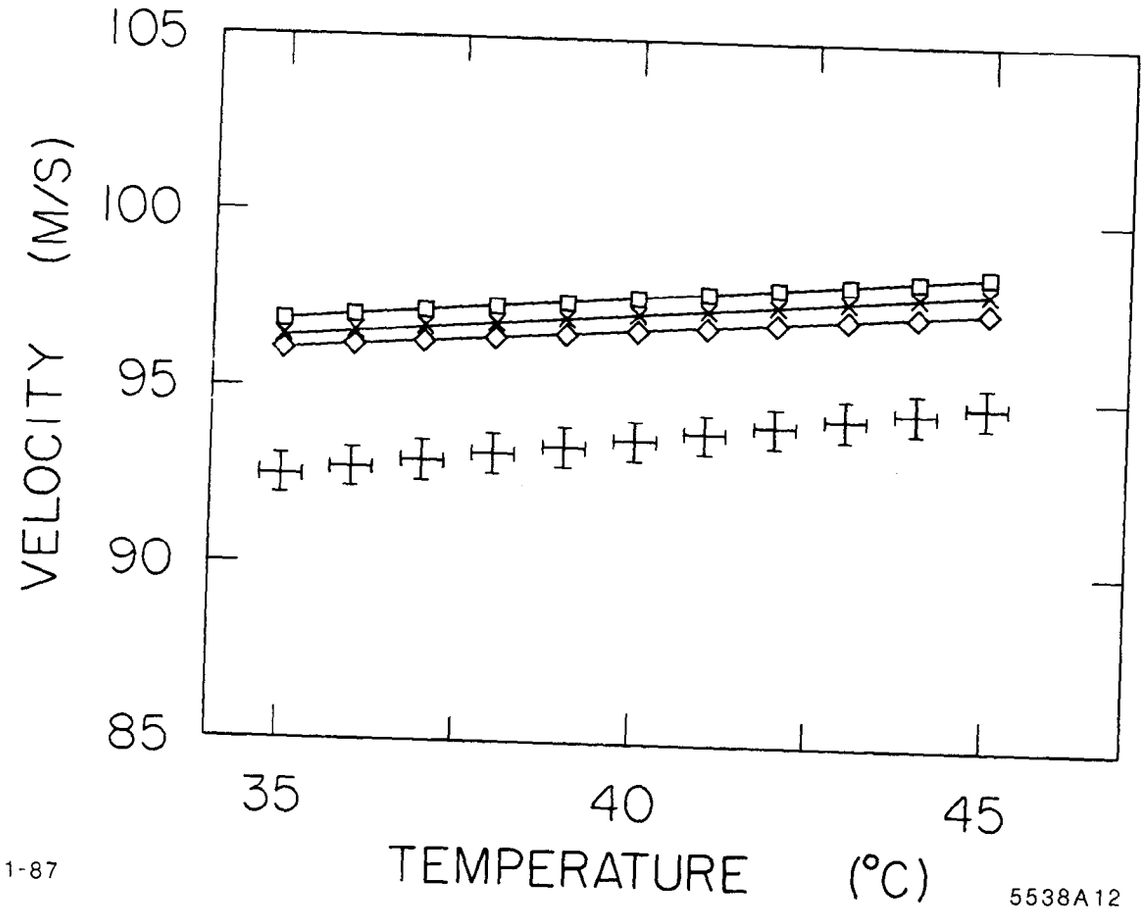
105
100
95
90
85
VELOCITY (M/S)
35
40
45
TEMPERATURE (°C)
1-87
5538A12

Fig. 10

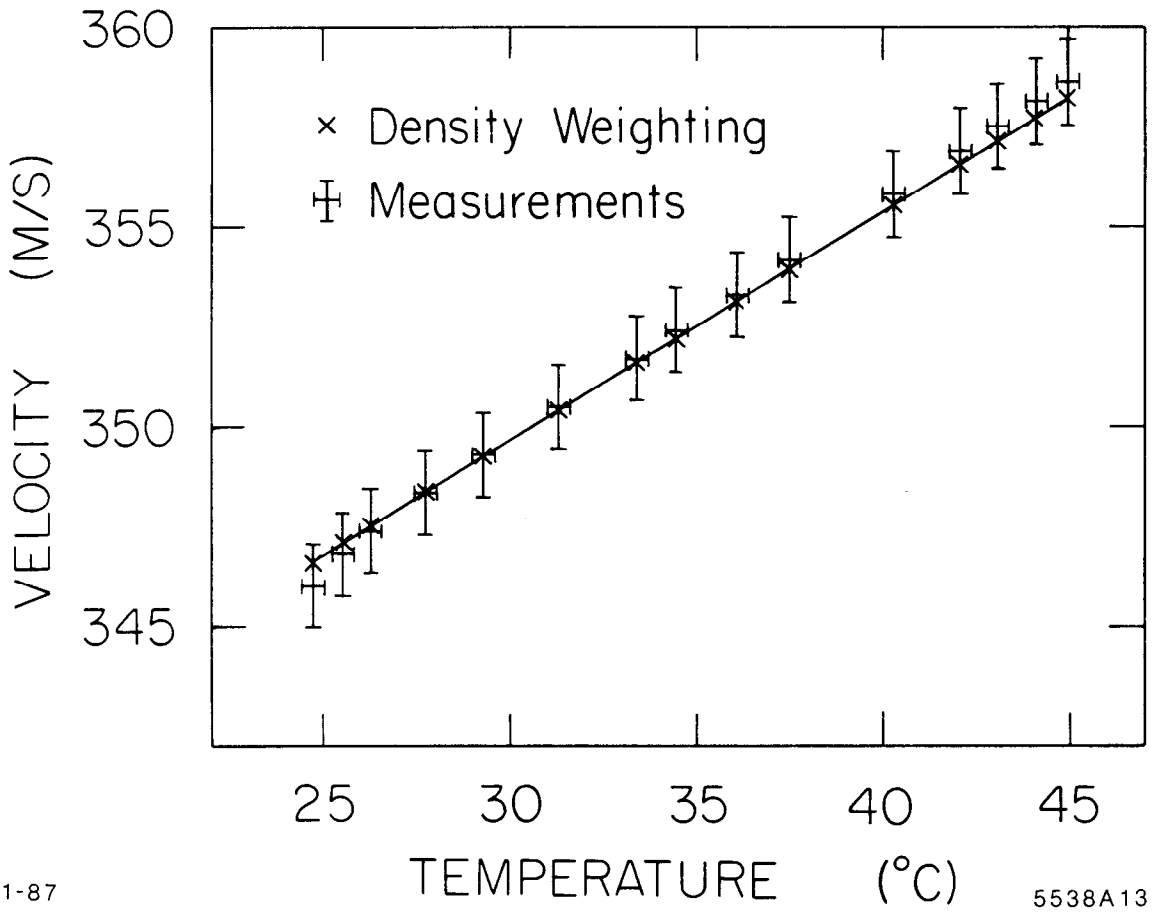
360
355
350
345
VELOCITY (M/S)
× Density Weighting
Measurements
25
30
35
40
45
TEMPERATURE (°C)
1-87
5538A13

Fig. 11

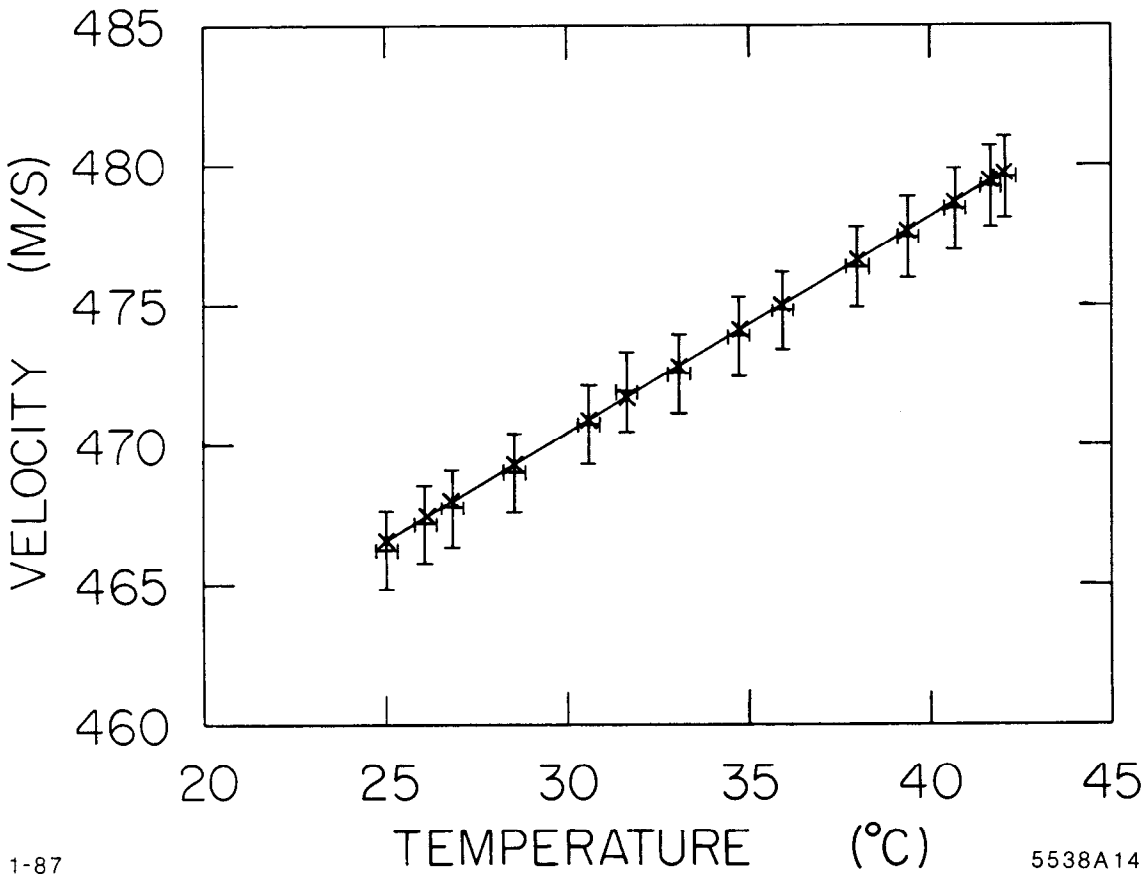
485
480
475
470
465
460
VELOCITY (M/S)
20
25
30
35
40
45
TEMPERATURE (°C)
1-87
5538A14

Fig. 12

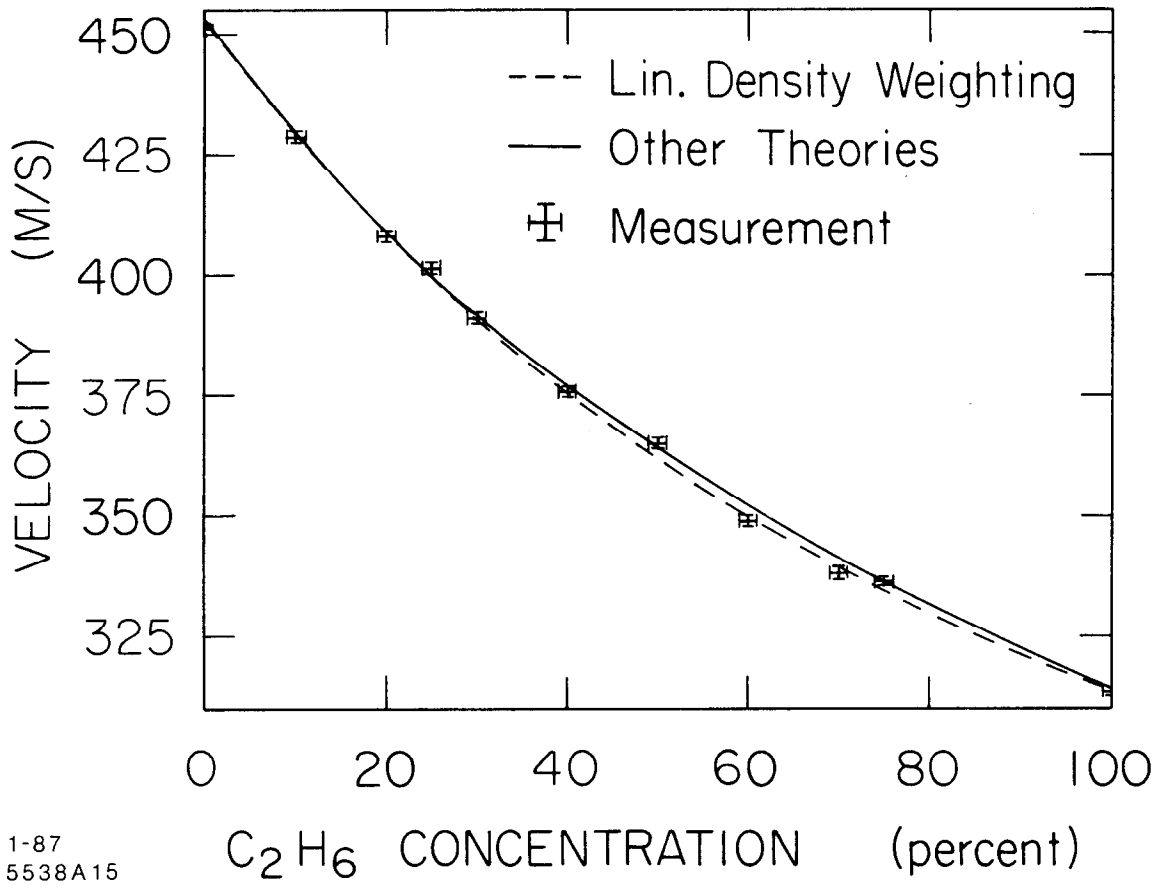
450
425
400
375
350
325
VELOCITY (M/S)
--- Lin. Density Weighting
—— Other Theories
Measurement
0
20
40
60
80
100
C_2H_6 CONCENTRATION (percent)
1-87
5538A15

Fig. 13

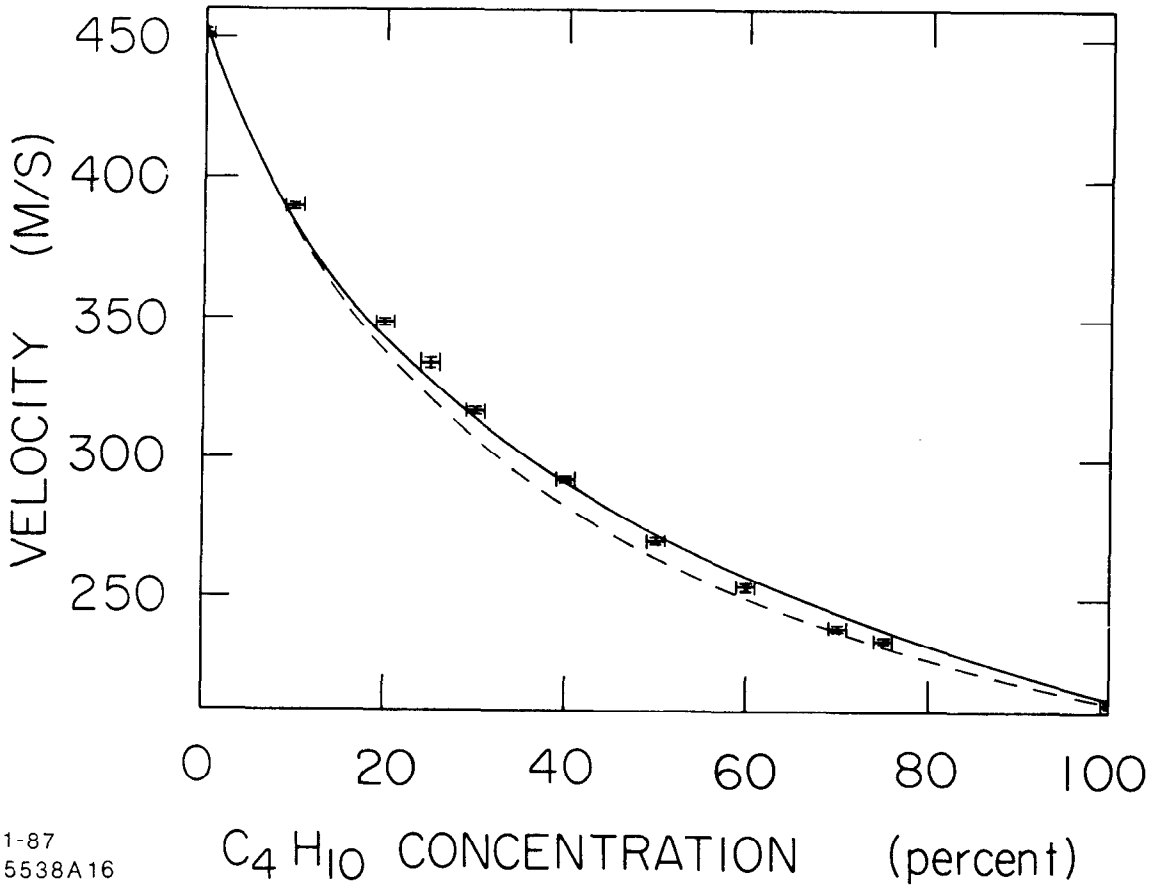
450
400
350
300
250
VELOCITY (M/S)
0
20
40
60
80
100
1-87
5538A16
$C_4 H_{10}$ CONCENTRATION (percent)

Fig. 14

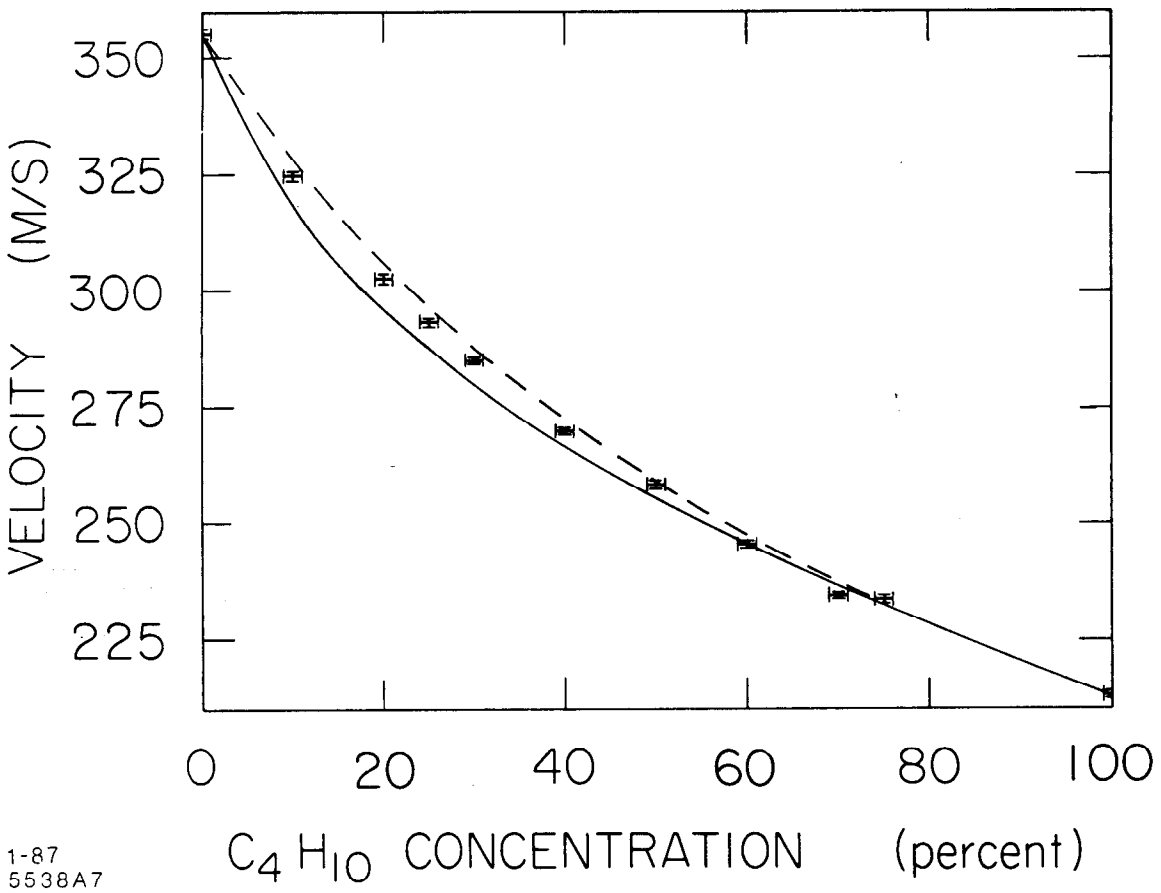
VELOCITY (M/S)
350
325
300
275
250
225
0
20
40
60
80
100
$C_4 H_{10}$ CONCENTRATION (percent)
1-87
5538A7

Fig. 15

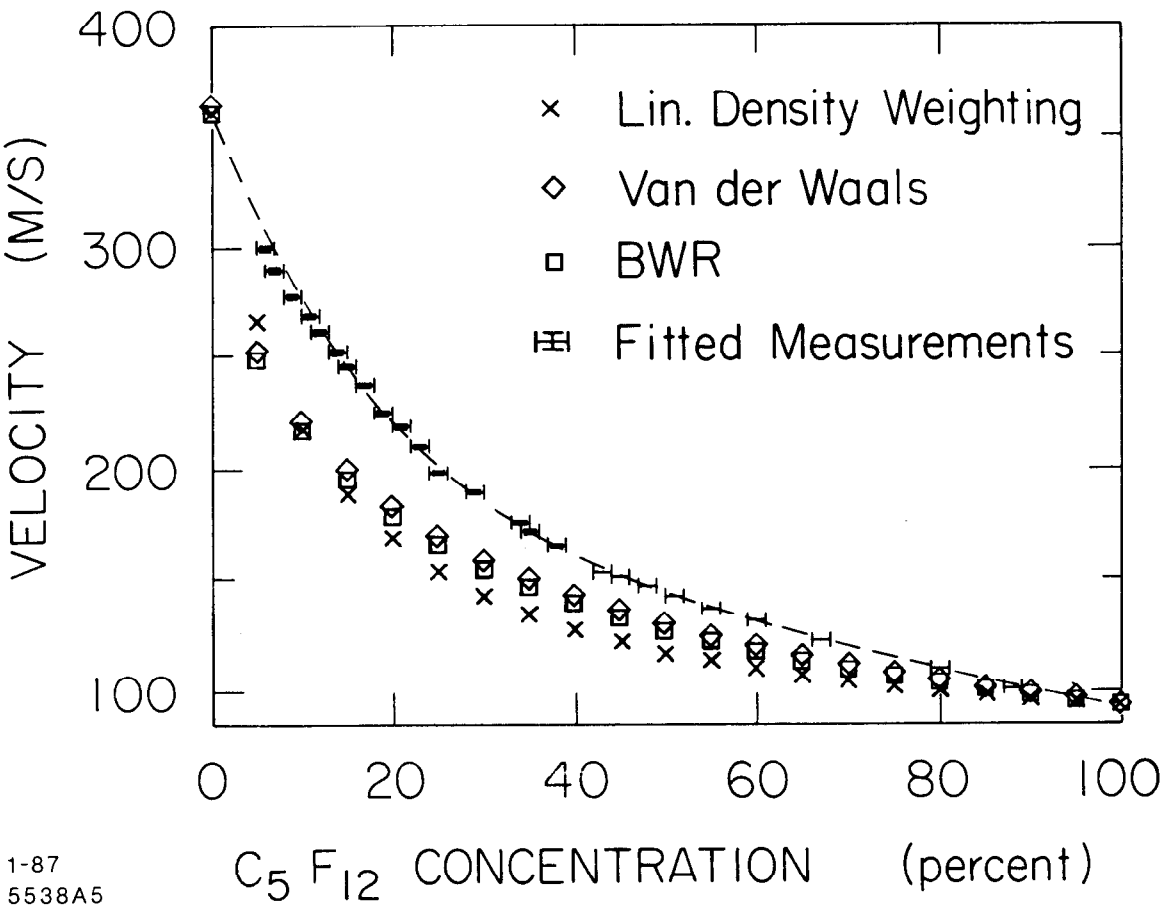
400
300
200
100
VELOCITY (M/S)
0
20
40
60
80
100
$C_5 F_{12}$ CONCENTRATION (percent)
Lin. Density Weighting
Van der Waals
BWR
Fitted Measurements
1-87
5538A5

Fig. 16